Nanoscale

REVIEW

View Article Online
View Journal | View Issue

Check for updates

Cite this: *Nanoscale*, 2022, **14**, 15242

Emerging SERS biosensors for the analysis of cells and extracellular vesicles

Mohammad Tavakkoli Yaraki, Anastasiia Tukova and Yuling Wang *

Cells and their derived extracellular vesicles (EVs) or exosomes contain unique molecular signatures that could be used as biomarkers for the detection of severe diseases such as cancer, as well as monitoring the treatment response. Revealing these molecular signatures requires developing non-invasive ultra-sensitive tools to enable single molecule/cell-level detection using a small volume of sample with low signal-to-noise ratio background and multiplex capability. Surface-enhanced Raman scattering (SERS) can address the current limitations in studying cells and EVs through two main mechanisms: plasmon-enhanced electric field (the so-called electromagnetic mechanism (EM)), and chemical mechanism (CM). In this review, we first highlight these two SERS mechanisms and then discuss the nanomaterials that have been used to develop SERS biosensors based on each of the aforementioned mechanisms as well as the combination of these two mechanisms in order to take advantage of the synergic effect between electromagnetic enhancement and chemical enhancement. Then, we review the recent advances in designing label-aided and label-free SERS biosensors in both colloidal and planar systems to investigate the surface biomarkers on cancer cells and their derived EVs. Finally, we discuss perspectives of emerging SERS biosensors in future biomedical applications. We believe this review article will thus appeal to researchers in the field of nanobiotechnology including material sciences, biosensors, and biomedical fields.

Received 31st May 2022,
Accepted 16th September 2022

DOI: 10.1039/d2nr03005e

rsc.li/nanoscale

Published on 19 September 2022. Downloaded on 2026-01-07 6:31:26 nm..

School of Natural Sciences, Faculty of Science and Engineering, Macquarie University, Sydney, NSW 2109, Australia. E-mail: yuling.wang@mq.edu.au

Mohammad Tavakkoli Yaraki

Dr Mohammad Tavakkoli Yaraki is a postdoctoral research fellow in the School of Natural Sciences, Macquarie University, Australia. He is an alumnus of the National University of Singapore, where he received his PhD in plasmon-enhanced processes for the diagnosis and therapy of cancer in 2020. His expertise is in the synthesis of metal nanostructures, synthesis of fluorescent nanomaterials, optical biosensors, and plasmon-enhanced processes including metal-enhanced fluorescence, metal-enhanced singlet oxygen generation and surface-enhanced Raman scattering. He has published 45+ papers in the area of nanobiotechnology and has 11+ years of experience in doing research in both academia and industry as well as entrepreneurship.

Anastasiia Tukova

Anastasiia received her B.Sc. in chemical engineering from St Petersburg State Chemical-Pharmaceutical University (Russia, 2016). She continued her M.Sc. in chemical and biomolecular engineering at the University of Sydney (Australia, 2018). In 2021, Anastasiia joined Yuling Wang's research group at Macquarie University. She started her PhD with a project that aimed to analyse how gold nanoparticles fundamentally interact with proteins via *advanced characterization of gold nanoparticles and their toxicological profile to control their biological behaviour and properties.*

This journal is © The Royal Society of Chemistry 2022

Published on 19 September 2022. Downloaded on 2026-01-07 6:31:26 nm..

1. Introduction

Raman spectroscopy is a spectroscopic technique that is based on the inelastic scattering of photons that cause vibration of chemical bonds in the molecules, first predicted theoretically in 1923 by Smekal and co-workers[1] and discovered by C.V. Raman in 1928, which led to a Nobel Prize in physics for Raman in 1930.[2] The rich vibrational information on changes in composition, structure, or phase transitions in the sample provided by Raman spectroscopy has made it a unique approach in analytical chemistry. However, Raman signals for bulk (solid) or concentrated samples are not strong enough for further analysis. Therefore, development of new techniques to enhance the Raman signal for a sample at low concentration is essential for further applications, especially in the biomedical field.[3–5]

Surface-enhanced Raman scattering (SERS), which was first discovered by Fleischmann *et al.*[6] in 1974, is a technique in which the Raman signal of a molecule can be enhanced dramatically when placed in the vicinity (<10 nm) of some nanomaterials including plasmonic noble nanostructures, 2D nanomaterials, and semiconductors. In general, there are two main mechanisms for SERS: (i) the plasmon-enhancement mechanism, which is the dominant mechanism in noble metal-based SERS systems, and (ii) the chemical enhancement mechanism, which is the main mechanism in non-metal-based SERS systems and also occurs between molecules and the substrate. In the last decade, colloidal and planar SERS systems have found their place as strong analytical tools in biomedical field[7–11] owing to their high sensitivity, which can be even at the single molecule level.[12]

Accurate analysis is imperative to inform health care providers in predicting the progression of a disease and implementing appropriate treatment. Biosensors can be used to observe and predict a patient's state of health by monitoring the presence of biomarkers in biological fluids such as blood, saliva and urine, tears, and cerebrospinal and synovial fluids.[13–19] Extensive research has been done on the use of analytical methods to monitor biomarkers such as circulating tumour cells (CTC), specific proteins, circulating RNA and DNA, and small extracellular vehicles (EVs)[20–26] to create fast, effective, and reliable assays and techniques to determine their activity and measure their concentration in patients' samples.[27–29] Among them, SERS-based systems have received tremendous attention owing to their high sensitivity and low signal-to-noise ratio background, as well as their non-invasive nature and requirement for a very low amount of sample.[10,30–32] Additionally, SERS biosensors could enable multiplex detection of various analytes in the sample by one single measurement, owing to the unique distinct Raman peaks of Raman reporter molecules in the design of SERS nanotags. Plenty of excellent reviews have been recently published on this topic.[33–35] However, it seems the chemical mechanism in SERS enhancement mechanism has been neglected, and no review specifically covers the use of SERS to analyse the surface biomarkers on cells and their EVs.

In this review, we first present an overview of SERS mechanisms with the focus on the chemical mechanism, which has been overlooked by many review articles. Then, we highlight different nanomaterials that have been used to design highly sensitive colloidal and planar SERS systems based on electromagnetic enhancement mechanism and chemical enhancement mechanism. Next, we discuss label-free and labelled SERS systems as two main approaches for the analysis of cancer cells and EVs, where various SERS systems based on plasmon enhancement and/or chemical enhancement have been designed to provide deeper insights into the molecular signatures of cells and EVs, and therefore for early detection or monitoring of the cancer treatment process. At the end, we propose our perspectives and future work using SERS as a sensitive tool for sensing cells and their EVs.

Yuling Wang

A/Prof. Yuling Wang is an Australian Research Council (ARC) Future Fellow in the School of Natural Sciences at Macquarie University. Yuling completed her PhD at the Chinese Academy of Sciences in 2009. She was then awarded an Alexander von Humboldt (AvH) fellowship (2010) and a German Research Foundation (DFG) fellowship (2012). In 2014, she received the ARC Discovery Early Career Researcher Awards fellowship. In 2017, Yuling was appointed as a Senior Lecturer at Macquarie and was promoted to Associate Professor in 2020. Her research focuses on platform technology that utilizes rationally designed plasmonic nanomaterials and surface-enhanced Raman scattering (SERS) for biomarkers sensing with the aim to enhance in vitro *diagnostics and personalized medicine.*

2. Overview of the SERS mechanism

The weak Raman scattering cross-section of molecules (10^{-28}–10^{-30} cm^2 per molecule) results in an inefficient Raman scattering, which has limited its application in real practice.[36,37] SERS has solved this issue by enhancing the Raman signal of molecules placed in the vicinity of SERS nanomaterials (*e.g.*, plasmonic nanostructures, semiconductors, *etc.*). Although the understanding of SERS enhancement has been one of the main topics in SERS studies for decades, debate about the mechanisms of SERS remains. Despite the many proposed models for SERS enhancement, there is still a need for a new SERS enhancement model to explain some complex systems. Fig. 1 shows the two common mechanisms that could be used to explain SERS enhancement in most systems based on different nanomaterials: (i) electromagnetic enhancement

Published on 19 September 2022. Downloaded on 2026-01-07 6:31:26 nm..

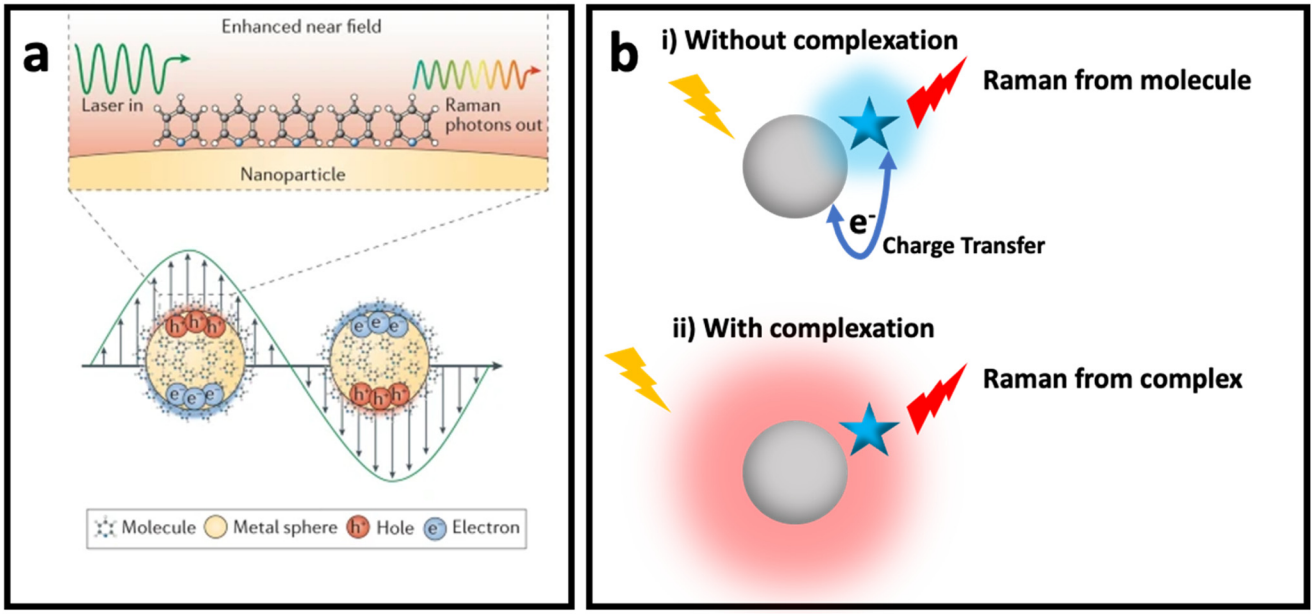

Fig. 1 (a) Enhanced near field in a plasmonic nanomaterial due to localized surface plasmon resonance (LSPR) when it interacts with incident light with wavelength larger than its size (bottom) and SERS of a molecule placed on surface of the plasmonic nanomaterials due to electromagnetic enhancement mechanism (top). Adapted from ref. 38 with permission from Nature-Springer Group, copyright 2016. (b) Chemical enhancement mechanism with macroscopic (without complexation) and microscopic (with complexation and formation of new electronic state) point of view when a molecule (blue star) is adsorbed on surface of a nanomaterial (grey sphere).

(Fig. 1a, *i.e.*, plasmon enhancement); and (ii) chemical enhancement (Fig. 1b with the two concepts of Macroscopic, where the charge transfer between nanomaterial (metal) and molecule occurs, and Microscopic, where nanomaterial and molecule form a complex with a new electronic energy state). In this section, these two main mechanisms are explained and the effective parameters of these mechanisms are reviewed.

2.1. Electromagnetic enhancement mechanism

Electromagnetic enhancement is the result of localized surface plasmon resonance (LSPR). When light (*i.e.*, electromagnetic wave) interacts with a metal or semiconductor nanostructure, oscillation of electrons at the surface of the metal or semiconductor nanostructure results in an enhanced electric field in the space surrounding the nanostructure, which can modulate the optical properties of molecules placed in the vicinity of the surface of the nanostructure, including Raman scattering.[7]

Noble metal (*i.e.*, Au, Ag, Pd, Pt, Cu) nanostructures have free electrons at their surface which lead to a considerably enhanced electric field in the surrounding environment, while the LSPR, and consequently the enhanced electric field under visible range excitation in semiconductors, is weak, since it depends on the electron density of the conduction band (CB) and a large electron density (10^{22}–10^{24} cm^{-3}) of the valence band (VB).[39] Therefore, the electromagnetic enhancement mechanism usually refers to noble metal-based SERS systems. Mie theory explains that when incident light with a certain wavelength is much greater than the size of nano-object, incident light interacts with a metal nanosphere, and the extinction cross-section in the nanosphere can be explained by the following equation:

$$\sigma_{ext} = 9\left(\frac{\omega}{c}\right)(\varepsilon_{diel})^{\frac{2V}{3}}\frac{\varepsilon''_{metal}}{(\varepsilon'_{metal}+2\varepsilon_{diel})^2+(\varepsilon_{metal})^2} \quad (1)$$

where V is volume of the sphere, w is the frequency of the incident light, ε_{dial} is the dielectric constant of the surrounding environment and ε''_{metal} and ε'_{metal} are the imaginary and real part of the refractive index of metal.[40–42] The SERS enhancement factor is proportional to the fourth power of enhanced electric field $\left(\frac{|E|^4}{|E_0|^4}\right)$. The enhanced electric field around metal nanostructures possesses short decay (10–30 nm in sphere and <10 nm in anisotropic nanoparticles with sharp edges and corners) (Fig. 2a), but when a dramatically enhanced electric field occurs in the space between the particles, this is called a "hot-spot" (Fig. 2b).[43–45,46] Therefore, the SERS enhancement factor is roughly proportional to d^{-12}, where d is the distance between the molecule and the surface of the metal nanostructure.[5] The enhanced electric field is size and shape dependent, and the material of the nanoparticle strongly affects the enhanced electric field. Therefore, appropriately matching the shape, size, and material of the nanoparticle with the excitation wavelength of the Raman scattering is of great importance for SERS applications. Fig. 2c shows how tuning the size of silver nanocubes affects the average enhanced electric field on the surface of these nanostructures under a common laser with the excitation wavelength. Although it was mentioned that semiconductors do not have

 This journal is © The Royal Society of Chemistry 2022

Published on 19 September 2022. Downloaded on 2026-01-07 6:31:26 nm..

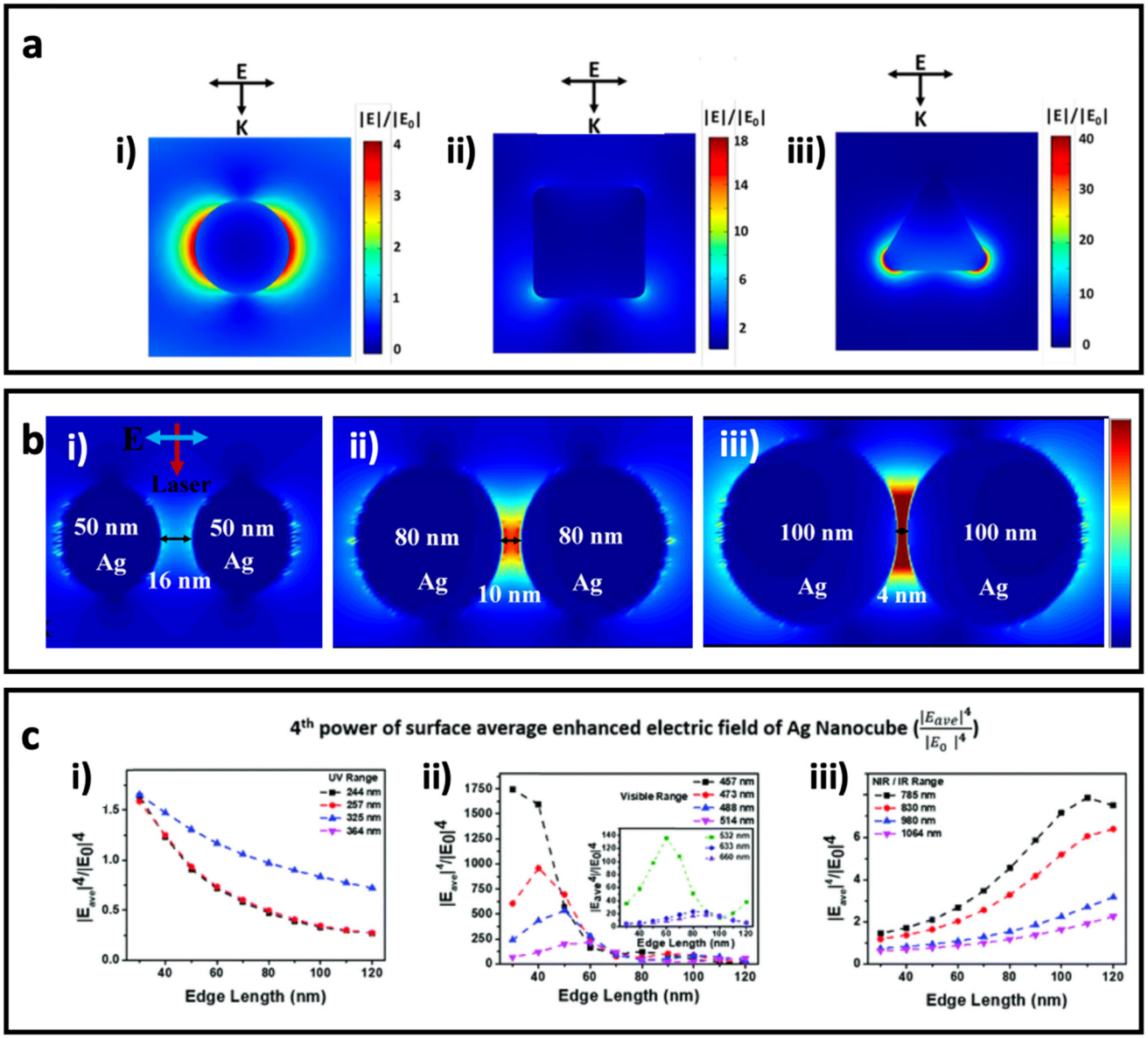

Fig. 2 (a) Enhanced electric field distribution around a 130 nm Ag sphere (i), 84 nm Ag nanocube (ii) and 33 nm Ag triangle nanoplate with 7 nm thickness (iii) under excitation wavelength of 550 nm, which is well matched with the maximum LSPR of each nanoparticle. Adapted from ref. 50 with permission from WILEY-VCH Verlag GmbH & Co. KGaA, Weinheim, copyright 2020. (b) The enhanced electric field between AgNPs with different sizes and gaps under 633 nm incident light, adapted from ref. 46 with permission from Nature-Springer Group, copyright 2019. (c) The fourth power of surface average enhanced electric field ($|E_{ave}|^4/|E_0|^4$ on Ag nanocubes with different sizes (based on edge length) under a common Raman laser with the excitation wavelength in the (i) UV region (200–400 nm), (ii) visible region (400–700 nm), and (iii) NIR/IR region (700–1100 nm). Adapted from ref. 45 with permission from the Royal Society of Chemistry, copyright 2020. ***K*** is the wave vector, and ***E*** is the incident polarization.

strong LSPR, and therefore they do not have a strong enhanced electric field in the visible region, some attempts have been made to shift the LSPR of semiconductor-based SERS systems to the visible range by optimizing the size and geometry configurations as well as defect engineering in the semiconductor nanomaterials. It should be taken into account that the LSPR peak is a function of the morphology (size and shape) and the component of the nanoparticle. There is an optimal size of metallic nanoparticles to achieve the strongest SERS enhancement. Small nanoparticles (<10 nm) have an extreme surface damping, while large nanoparticles have a great radiation damping (>160 nm).[47] It is important to note that for a different excitation wavelength the choice of optimal nanoparticle size for maximum SERS enhancement will vary. Surface plasmons are also strongly influenced by the shape of nanoparticles. For example, gold nanorods have two resonance modes at different wavelengths corresponding to the longitudinal and transverse direction of plasmon oscillation.[48]

Published on 19 September 2022. Downloaded on 2026-01-07 6:31:26 nm..

Adjusting the aspect ratio of these nanoparticles would result in shifting of the LSPR peak, and as a result in different SERS enhancement. LSPR and SERS enhancement also depend on the surrounding environment. For example, Li *et al.* have investigated the optimal size of gold nanoparticles for SERS under different conditions.[49] They found that under the same concentration and total surface area of gold nanoparticles the optimal size for the maximum SERS enhancement among the particles from 17 to 80 nm is 50 nm. SERS also depends on the component of NPs. Although Ag exhibits high plasmonic quality in the visible to near-infrared range and enhances strong Raman scattering, chemical stability and toxicity are two major concerns for its biomedical applications. Au exhibits SERS enhancement comparable to Ag in the long wavelength range (usually above 600 nm), but gold is widely used due to its high chemical stability and biocompatibility.

2.2. Chemical enhancement mechanism

Although electromagnetic enhancement usually occurs in metal nanostructure-based SERS systems and is the dominant mechanism, chemical enhancement is the dominant mechanism when a molecule locates on the surface of a semiconductor (metal oxides) or non-metal nanostructure (carbon nanomaterials).[9,51] In chemical enhancement, the charge transfer process occurs between the metal or non-metal substrate and adsorbed molecule (Fig. 3a). This charge transfer process can happen in two different ways depending on the electronic states of the nanomaterial (SERS substrate) and the adsorbed molecule.[52–54] First, the substrate and molecule may form a complex that has a new energy state, where the resonance of such a complex could enhance the Raman scattering under excitation by incident light. Second, there is no complex state, but the Fermi level of the nanomaterial substrate could match the highest occupied molecular orbital (HOMO) or the lowest unoccupied molecular orbital (LUMO) of the molecule. In this case, the electron can be transferred from the HOMO of the molecule to the unoccupied state above the Fermi level of the nanomaterial substrate, or from the LUMO of the molecule to the occupied state below the Fermi level of the nanomaterial substrate. A third possible pathway is excitation resonance, which is different from charge transfer system and happens when excitons (*i.e.*, electron–hole pairs) are being generated as a result of electron transition from valence band to conductive band. When the size of nanoscale semiconductor is smaller than the distance between hole and pair (*i.e.*, Bohr radius), the bandgap increases. If the wavelength of incident light is matched with the bandgap energy, the SERS performance of semiconductor nanoparticles through the chemical enhancement effect (*i.e.*, exciton resonance) can be improved.[55,56]

2.3. Synergic effect between electromagnetic enhancement and chemical enhancement mechanisms

The combination of the two mechanisms, taking advantage of the synergic effect between the two well-known mechanisms, in developing SERS substrates has been one of the hot topics in this research area. While surface defect-engineered semiconductors have been used as potential SERS substrates for some biomedical applications,[57–59] it seems that the application of semiconductor nanomaterials in bioanalysis needs further investigation to solve the practical challenges that researchers face in biomedical applications, in particular in the analysis of cells and extracellular vesicles. Therefore, the combination of noble metal nanostructures and semiconductor nanomaterials has received tremendous attention in the design of SERS substrates with stronger SERS effect compared with noble metal-based substrates or semiconductor-based substrates alone.[60–64] In such a composite, the presence of a noble metal results in stronger light absorption in the visible to near-infrared (NIR) region, depending on the size/shape/material of the noble metal nanostructure. This can modify the light absorption of the composite and lead to stronger excitation under Raman laser irradiation. On the other hand, since semiconductors have a generally higher Fermi level than noble metal nanostructures, the hole–electron separation effect in a semiconductor can be promoted by the presence of the metal nanostructure, and therefore the charge transfer efficiency of the semiconductor can be improved. Fig. 3b depicts how the combination of Au and TiO_2 nanostructures could enhance the Raman signal. In this work,

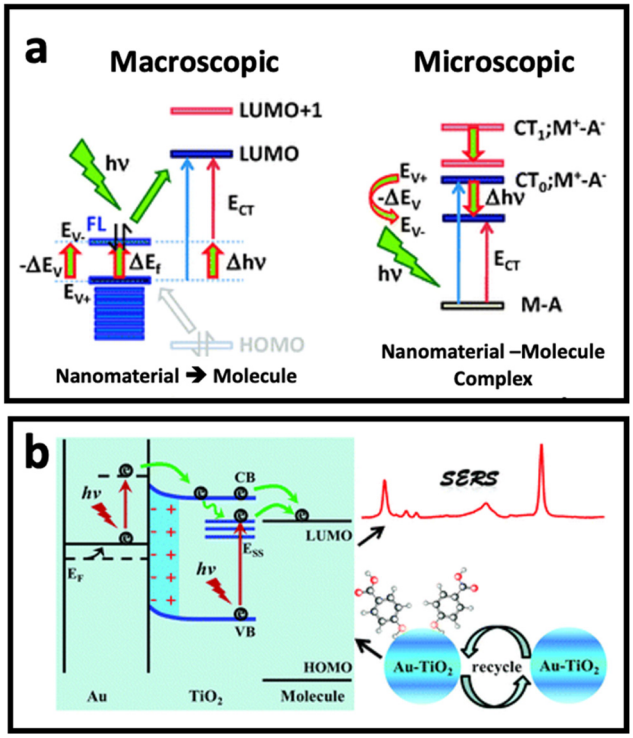

Fig. 3 (a) Chemical enhancement mechanism based on resonant charge transfer model with macroscopic and microscopic point of view when a molecule is adsorbed (A: adsorbate) on surface of nanomaterial (in this case M: metal). Adapted from ref. 68 with permission from the Royal Society of Chemistry, copyright 2011. (b) Schematic diagram of the SERS enhancement mechanism of 4-mercaptobenzoic acid (4-MBA) molecules adsorbed on Au–TiO_2 nanocomposite. Adapted from ref. 65 with permission from the Royal Society of Chemistry, copyright 2017.

This journal is © The Royal Society of Chemistry 2022

Published on 19 September 2022. Downloaded on 2026-01-07 6:31:26 nm..

Jiang *et al.*[65] deposited Au ions on TiO_2 nanoparticles by a photocatalytic reduction approach, where it was found that a synergic effect between deposited Au and TiO_2 nanoparticles plays an important role in the enhanced charge transfer from semiconductor to the adsorbed 4-mercaptobenzoic acid molecules, and in turn, the SERS effect of the nanocomposite. The synergistic effect between electromagnetic mechanism and chemical enhancement is not limited to metal–semiconductor substrates. Recently, MXenes made of Ti_3C_2, Nb_2C, and Ta_2C have shown up to 10^6-fold SERS enhancement factor, which was due to a combination of both enhanced electric field around the MXene structures and charge transfer between MXene and Raman molecule.[66,67] We believe these nanomaterials have great potential for the analysis of surface biomarkers on cells or extracellular vesicles in the near future.

To date, the potential of a wide range of nanomaterials for SERS enhancement has been investigated. Plasmonic noble nanostructures have shown promising SERS enhancement effects in both colloidal and planar systems through the electromagnetic enhancement (*i.e.*, plasmon enhancement) mechanism. While chemical enhancement has also been found in metals, it is suppressed by the electromagnetic enhancement mechanism. However, in non-plasmonic nanomaterials such as semiconductors and 2D carbon nanostructures, the chemical enhancement effect is the dominant mechanism, and mainly occurs through the charge transfer process. Combination of these nanomaterials provides an opportunity to take advantage of the synergic effect between metal and non-metal nanomaterials, and to obtain dramatic SERS enhancement. In the following section, we discuss the nanomaterials that contribute to SERS enhancement *via* these mechanisms.

3. Nanomaterials for SERS

3.1. Nanomaterials for the plasmon enhancement effect

Noble metal nanostructures are the key nanomaterials that have been used for designing SERS systems in both colloidal and planar systems owing to their LSPR effect, and in turn, the dramatically enhanced electric field in their surrounding environment. As discussed earlier, the Raman signal of the molecule can be modulated when it is placed in this enhanced electric field area (*i.e.*, typically the molecule is adsorbed on surface of metal nanostructure), which is proportional to the fourth power of the enhanced electric field. Among various noble metals, gold and silver have received more attention compared with other plasmonic metals (*i.e.*, Cu, Pd, Pt), owing to their well-known size and shape-tunable chemical synthesis routes (*i.e.*, bottom-up approaches), as well as the fewer technical challenges in the fabrication of nanostructures *via* top-down approaches (*e.g.*, electrodeposition). In this section, we highlight nanomaterials that have been used for designing colloidal and planar SERS systems based on the plasmon enhancement mechanism.

3.1.1. Colloidal SERS systems with plasmon enhancement effect. Synthesis of metal nanoparticles with a size less than 100 nm is at the heart of development of SERS systems in colloidal form. Since the enhanced electric field is stronger at sharp edges and corners in anisotropic metal nanoparticles, the development of reproducible synthesis routes for anisotropic metal nanoparticles is of great importance. The synthesis of anisotropic gold and silver nanoparticles has been recently reviewed by different groups.[69–73] In general, the successful synthesis of anisotropic metal nanoparticles requires the presence of metal salt (*i.e.*, mostly $HAuCl_4$, $AgNO_3$), mild reducing agent (*i.e.*, ascorbic acid, hydroquinone, *etc.*) and shape-directing agent (*i.e.*, polymers and a trace amount of ions). The morphology and size of the anisotropic metal nanoparticles can be controlled *via* two general ways: direct (seedless) synthesis and seed-mediated growth, shown schematically in Fig. 4a.

In direct synthesis (Fig. 4a, left), a combination of mild reducing agent and shape-driving agent can lead to the formation of anisotropic nanoparticles, where bio-templated/biomolecules-based methods can satisfy these requirements. Biomolecules such as peptides, proteins and nucleic acids, proteins and peptides as well as plant extracts containing bioactive compounds could be used for the synthesis of anisotropic nanoparticles, due to the simultaneous presence of various sequences (*i.e.*, nucleotides or amino acids) or chemical structures.[78–80] For example, Tan *et al.*[81,82] have reported the synthesis of triangular Au nanoplates using polypeptide as simultaneous reducing agent, shape-directing agent and capping agent under mild synthesis conditions such as neutral pH, room temperature and in aqueous solution. The as-synthesized nanostructures through these routes are fully covered with functional groups that enable further surface functionalization easily and provide high biocompatibility, which are essential for biomedical applications.[83–85] In another study, Wang's group reported the seedless synthesis of spiky Au nanostars using ascorbic acid as reducing agent and capping agent in the presence of a trace amount of Ag^+ ions as shape-directing agent, which showed a great SERS enhancement.[86] In another work, using the same precursors, and just by changing the ratio between chemicals and synthesis conditions, Au–Ag alloy nanoboxes with a relatively smooth surface were synthesized.[87]

On the other hand, the seed-mediated growth approach (Fig. 4a, right) allows the manipulation of the shape and size of the anisotropic nanoparticles by introducing different amounts of seeds (*i.e.*, usually small-sized nanoparticles with a size between 5 and 20 nm) as well as a shape-directing agent such as polyvinylpyrrolidone (PVP),[88] poly(diallyldimethylammonium) chloride (PDDA),[75] cetyltrimethylammonium bromide (CTAB),[89] and a trace amount of metal ions (Ag^+, Fe^{2+}, *etc.*).[50,90] The shape-directing agents usually have specific binding affinity for certain facets (*e.g.*, {100}, {111}) in the crystal structure of the seeds, leading to reducing of metal ions and growth of the nanoparticle in specific directions. A careful control of the ratio between the reagents in the synthesis can

Published on 19 September 2022. Downloaded on 2026-01-07 6:31:26 nm..

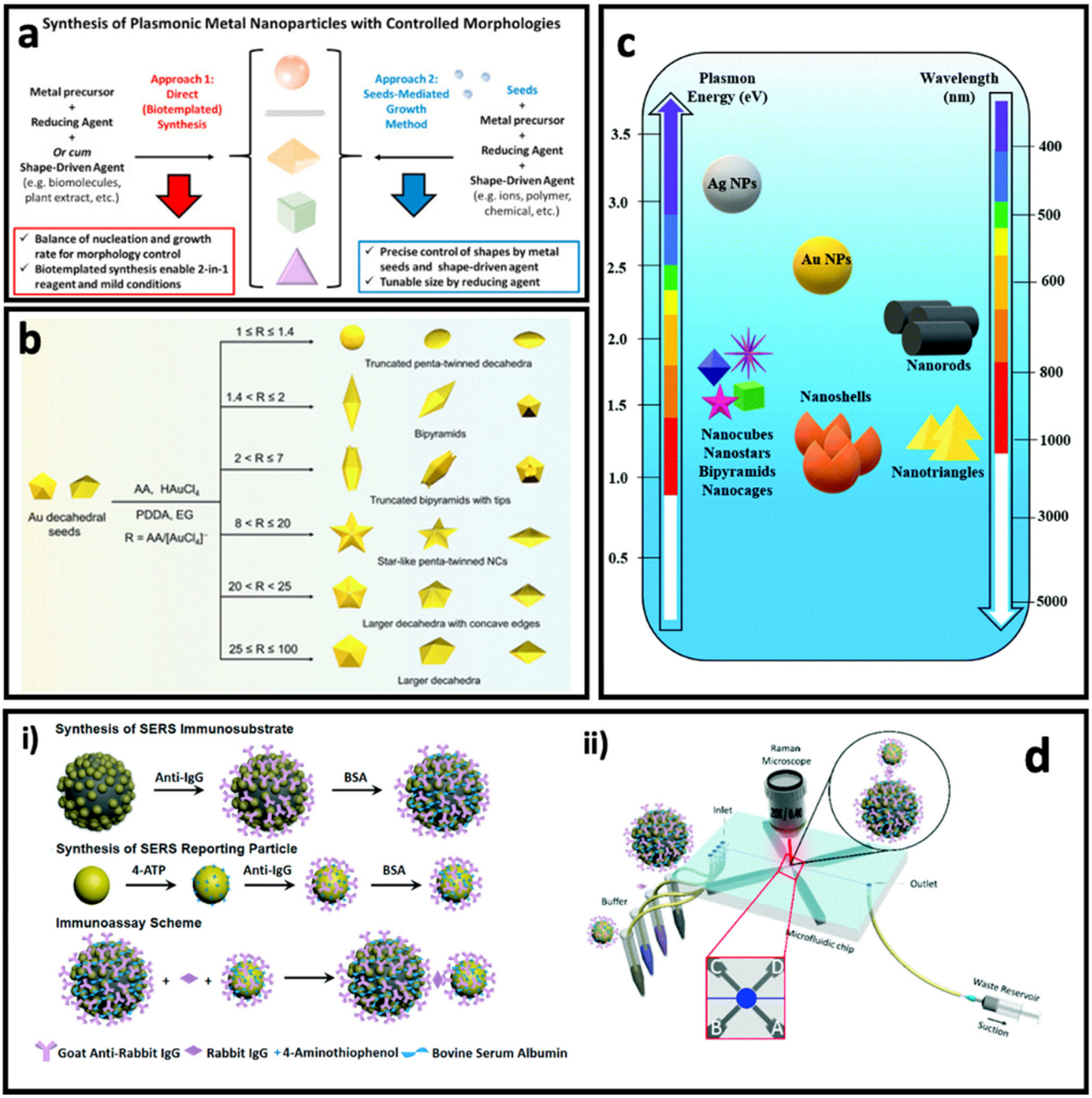

Fig. 4 (a) Controlling the morphologies of metal nanoparticles *via* two main approaches: direct (seedless) synthesis (left) and seed-mediated growth method (right). Adapted from ref. 74 with permission from Elsevier, copyright 2020. (b) Controlled synthesis of penta-twinned Au nanocrystals by tuning the ascorbic acid (AA)/$HAuCl_4$ ratio. Adapted from ref. 75 with permission from the Royal Society of Chemistry, copyright 2021. (c) Plasmon resonance and maximum LSPR peak of differently shaped gold (Au) and silver (Ag) nanoparticles (NPs). Adapted from ref. 76 with permission from the Royal Society of Chemistry, copyright 2021. (d) Synthesis of Fe_3O_4@AuNP@Ag as magnetic SERS nanotag (i) and its application in a microfluidics device for detection and quantification of immunoglobulin G. Adapted from ref. 77 with permission from the Royal Society of Chemistry, copyright 2017.

result in anisotropic nanoparticles with well-defined shapes. For example, Ag bipyramids have been synthesized in the presence of CTAB, ascorbic acid and Cu^{2+} ions, where CTAB was specific to {100} facets of Ag seeds, and the combination of ascorbic acid and Cu^{2+} ions produced H_2O_2 that could etch the {110} and {111} facets on Ag seeds.[50] Recently, Zhang *et al.*[75] reported the synthesis of penta-twinned Au nanocrystals using Au decahedral seeds (Fig. 4b). Au decahedral seeds were first synthesized using ethylene glycol as solvent, ascorbic acid as reducing agent and PDDA as shape-directing agent at 220 °C. Then, the seeds were used for the synthesis of various penta-twinned nanocrystals (truncated penta-twinned decahedra,

 This journal is © The Royal Society of Chemistry 2022

Published on 19 September 2022. Downloaded on 2026-01-07 6:31:26 nm..

truncated bipyramids, bipyramids, truncated bipyramids with tips, star-like penta-twinned nanocrystals, decahedra with concave edges, and decahedra) just by tuning the ascorbic acid/$HAuCl_4$ ratio in the presence of Ag^+ ions. As can be seen in Fig. 4c, different shapes of gold and silver nanoparticles have different LSPR peaks, and therefore the SERS enhancement factor is maximum when the laser wavelength is well matched with the LSPR peak of the nanoparticle.

One of the interesting approaches to improve the SERS intensity in colloidal SERS nanotags is aggregation-induced SERS.[91,92] In this approach, the SERS intensity increases dramatically due to formation of hot-spots between the SERS nanotags upon addition of the analyte.[93] For example, Liu *et al.* have used porous Au@ZnS multi-yolk–shell structures derived from Au@ZIF-8 as SERS nanotags, where introducing the electrolyte resulted in a dramatic enhancement of the SERS intensity of these nanoparticles due to aggregation of them.[94] This approach has also been used as the basis of a lot of magnetic bead–SERS nanotags biosensors. In this approach, both metal SERS nanotags and magnetic beads are functionalised by recognition elements that can interact with analyte molecules, resulting in the formation of magnetic bead/metal nanoparticles in the form of core/satellite shape. The metal nanoparticles (as satellites) in this structure become close enough to each other that many hot-spots are formed between them. In another method with a similar concept, magnetic SERS nanotags made of a magnetic core and grown metal nanoparticles on the surface can be designed.[95] For example, Yap *et al.*[77] designed Fe_3O_4@AuNP@Ag as magnetic SERS nanotags that were used to quantify immunoglobulin G protein using a microfluidic device (Fig. 4d). The external magnetic field causes the aggregation of the SERS nanotags, leading to a dramatic enhancement in SERS intensity.

3.1.2. Planar SERS systems with plasmon enhancement effect. Planar SERS systems are of interest for designing analytical tools, where the SERS substrates can be made *via* different approaches: (i) assembly of metal nanoparticles onto a substrate, and (ii) deposition of metal atoms on the surface of a substrate and formation of metal nanostructures. The substrate is usually a dielectric material such as glass, silicon wafer, paper, and polymer that has an inert effect and provides a versatile surface chemistry for further surface functionalization and binding of metal nanoparticles.

The assembly of metal nanoparticles onto the substrate can be performed *via* electrostatic adsorption, a simple casting/drying process, solvent-mediated, sputtering, or even chemical binding.[10] All these approaches usually result in a layer of metal nanoparticles on the surface of the substrate, where hot spots can be formed in the space between the metal nanoparticles.[100] Another approach to make SERS substrate using metal nanoparticles is by combining metal nanoparticles with polymers and casting the polymer solution as a thin film. The performance of the metal nanoparticle-based SERS substrate strongly depends on the surface coverage and shape of the metal nanoparticles. Solís *et al.*[96] have investigated the effect of surface coverage of spherical AuNPs, Au nanorods, and spiky Au nanostars on a glass substrate. As can be seen in Fig. 5a, the SERS enhancement factor is more sensitive to surface coverage in spherical nanoparticles than anisotropic nanoparticles, where the spiky Au nanostars showed less sensitivity. Additionally, the Au nanostars led to at least 1 order of magnitude higher SERS enhancement factor compared with spherical Au nanoparticles, which could be due to formation of stronger "hot-spots" between the sharp tips of the Au nanostars. In general, deposition of metal nanoparticles on substrates is an easy and cheap process; however, reproducibility of the quality of these SERS substrates should be considered in real biomedical applications.

Deposition of metal atoms on the surface of the substrate using atomic electrodeposition equipment through a lithographic approach or using a template is another technique that enables researchers to investigate the performances of SERS substrates with unique, well-defined structures for both in-plane and out-of-plane vertically stacked plasmonic nanogaps. For example, Hu *et al.*[97] have fabricated a flexible polymeric nanofinger coated with a thin layer of Au. As shown in Fig. 5b, the presence of the analyte molecule can bring the plasmonic nanofingers close to each other as result of capillary forces during the drying of the sample. This results in a dramatically enhanced electric field between the tips and, therefore, high SERS sensitivity. In another work, a dual-templating technique has been used to fabricate a 3D hierarchically porous gold nanostructure, by Zhang *et al.*[98] In this approach (Fig. 5c), porous poly(methyl methacrylate) (PMMA) and octaethylene glycol monohexadecyl ether ($C_{16}EO_8$) were used as hard template and lyotropic liquid crystal (LLC), respectively. A porous anodic aluminium oxide (AAO) template was used to prepare a negative PMMA template, followed by formation of LLC and, finally, electrodeposition of gold. The synthesized nano-holes could harvest the incident light and therefore generate an electric field enhancement close to the edges of the nano-holes. The fabricated substrate showed considerable reproducibility and sensitivity for detection of benzenethiol at ultralow concentrations (0.1 pM). Although this approach provides unique SERS substrates at laboratory scale, the cost and time for the preparation of this type of SERS-active substrate should be taken into account when the scaling up of this type of SERS substrate is required. In another study, an ultrathin plasmene nanosheet was fabricated by stamping Au@Ag nanocubes on different substrates including paper banknote, polymer banknote and coin (Fig. 5d). The stamped nanostructures have shown dramatic SERS enhancement for 4-ATP molecules (as model Raman molecule). Careful tuning of the morphology of the nanoparticles in this approach could be used as a method to engineer the SERS performance.[99] The self-assembly of nanoparticles on a flexible planar substrate has been reported in many studies.[101,102] Huang's group has reported a new fabrication method based on tailoring the contact angle of nanoparticles to assemble the nanoparticles instantly (within 5 s) on silicon wafer.[103] In another study, the same group has reported controlling the SERS intensity of a planar system (containing a monolayer of gold nanoparticles)

Published on 19 September 2022. Downloaded on 2026-01-07 6:31:26 nm..

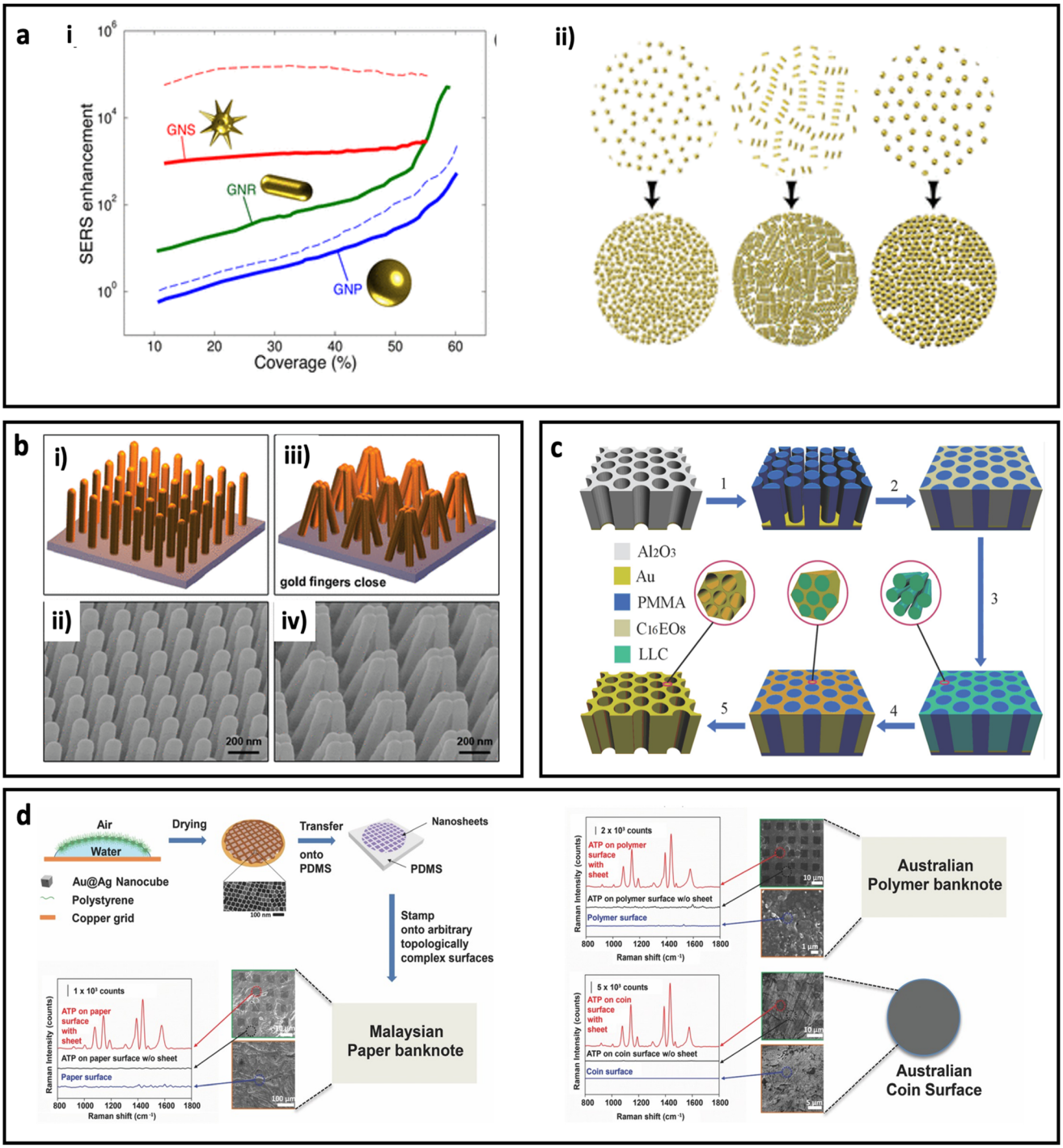

Fig. 5 (a) Effect of surface coverage on SERS enhancement in a metal nanoparticle-based substrate (i) and schematic illustration of change in density of nanoparticles with increasing the deposition time. Au nanoparticles (GNPs, 51 nm diameter), Au nanorods (GNRs, 65 nm length, 21 nm diameter), and Au nanostars (GNSs, core with 20 nm diameter and 10 branches 15.5 nm long with tip apexes of 1 nm), solid curves for 785 nm excitation laser wavelength and dash curves for 633 nm excitation laser wavelength. Adapted from ref. 96 with permission from the American Chemical Society, copyright 2017. (b) Schematic illustration of plasmonic nanofinger and its SEM image before addition of analyte (i and ii) and after drying of analyte (iii, and iv). Adapted from ref. 97 with permission from the American Chemical Society, copyright 2010. (c) Schematic illustration of different steps for preparation of 3D hierarchically porous gold nanostructure. Adapted from ref. 98 with permission from WILEY-VCH Verlag GmbH & Co. KGaA, Weinheim, copyright 2015. (d) Schematic illustration of fabrication procedure for adhesive plasmonic SERS substrate using Au@Ag nanocube and polydimethylsiloxane (PDMS) (top left) and application of the fabricated SERS substrates on Malaysian paper banknote (bottom left), Australian polymer banknote and Australian coin surface (right). 4-Aminothiophenol (ATP) was used as Raman reporter molecule. Adapted from ref. 99 with permission from WILEY-VCH Verlag GmbH & Co. KGaA, Weinheim, copyright 2015.

This journal is © The Royal Society of Chemistry 2022

Published on 19 September 2022. Downloaded on 2026-01-07 6:31:26 nm..

by adjusting the shrinkage of the substrate through light. In this design, the substrate was made by photopolymerization of acrylamide, which undergoes the photopolymerization process under irradiation of UV light.[101] This polymerization led to shrinkage of the substrate, and therefore the formation of hot-spots between nanoparticles that resulted in higher SERS intensity.[104]

3.2. Nanomaterials for the chemical enhancement effect

Although nanomaterials that have been used for developing SERS systems with the chemical enhancement effect are mostly based on inorganic semiconductors and carbon-based nanostructures (Table 1), metal nanoparticles have also shown the chemical enhancement effect when the adsorbed molecules experience the charge transfer to the metal surface. Since the plasmon effect is the dominant mechanism in metal nanoparticles, in this section, we only discuss the non-metallic nanostructures that have been used for designing SERS systems with the chemical enhancement effect. The first observation of SERS on TiO_2 and NiO by Yamada *et al.*[105,106] can be traced back to 1982, when they discovered the enhancement in Raman spectra of chemisorbed pyridine on the smooth surface of NiO-coated glass substrate. Since then, the research on using semiconductor nanomaterials as Raman enhancers has witnessed much progress, and various types of nanomaterials including metal oxides, single-element semiconductors, transition metal dichalcogenides, and organic semiconductors have been found as potential SERS substrates. In the following sections, we briefly review these nanomaterials and their applications as SERS substrates through the chemical enhancement mechanism.

3.2.1. Inorganic semiconductors. Inorganic semiconductor nanomaterials such as metal oxides and metal dichalcogenides have been used extensively for SERS. Metal oxides including TiO_2, ZnO, Cu_2O, Fe_2O_3, MoO_2, VO_2, WO_3, Ta_2O_5, and Nb_2O_5 are high refractive index semiconductors that have low cost, high chemical stability, high biocompatibility, high carrier mobility, are easy to prepare with high controllability and have shown high SERS reproducibility.[107–110] TiO_2 has been one of the most interesting metal oxides for researchers, due to its simple synthesis routes and low cost. Yang *et al.*[111] have investigated the effect of phase structure of TiO_2 on its SERS activity using 4-mercaptobenzoic acid (4-MBA) as Raman reporter. They found that an appropriate mixture of rutile and anatase phase is favoured to achieve maximum SERS enhancement. In another study, hydrogenated black TiO_2 nanowires were used to make SERS substrate (Fig. 6a), where it was found that hydrogenation is an effective method that could result in a 3-fold higher SERS enhancement factor.[112] Xue *et al.*[113] investigated the effect of crystallite size (*i.e.*, in the range of 6.8 nm–14.2 nm) on the SERS performance of TiO_2 nanoparticles. They found that nanoparticles with crystallite size of 10.9 nm have maximum SERS effect; this better performance can be attributed to the quantum confinement effect between TiO_2 nanoparticles and adsorbed 4-MBA molecules and improved charge-transfer resonance. After demonstration of the SERS activity of colloidal ZnO in 1996,[114] the SERS activity of different ZnO nanostructures has been examined. For example, submicron flower-shaped ZnO nanostructures were synthesized by Zhang *et al.*[115] and showed considerable SERS activity, to be employed as a biosensor for detection of heavy metal ions. Although most research is focused on TiO_2 and ZnO, the SERS activity of other metal oxides has also been examined. For example, amorphous Nb_2O_5 nanoflowers synthesized by the hydrothermal method have shown the chemical enhanced SERS effect under 532 nm excitation laser.[116] The as-synthesized nanostructures also possessed a crystal-dependent and thermally affected SERS performance, which is similar to what has been observed in other metal oxides.[111]

Since the SERS performance is usually weak (enhancement factor between 10^2–10^5) in pure semiconductors,[113,122,123,127] there are different strategies to engineer the bandgap of semiconductors, and in turn, improve their SERS effect through the chemical enhancement mechanism. Doping the structure of a semiconductor using a trace amount of another metal/non-metal is an effective strategy to engineer the bandgap of semiconductors. For example, Yang *et al.*[59] have reported the synthesis of Mo-doped Ta_2O_5 nanowires that were used to make a SERS substrate. The fabricated SERS substrate exhibited a remarkable SERS sensitivity with an enhancement factor of 2.2×10^7 using methyl violet (MV). This value is 1–2 orders of magnitude larger than the enhancement factor reported for other metal oxides.[133,134] Another approach is defect engineering by producing oxygen vacancies in the structure of semiconductors.[135–137] Various methods such as lithium metal grinding reduction, irradiation, and high-temperature annealing under a reducing gas atmosphere have been employed to generate oxygen vacancies in the structure of semiconductors.[138–141] For example, Cao *et al.*[140] have successfully synthesized MoO_{2-x} with a polycrystalline surface by

Table 1 Recent advances in nanomaterials for SERS through chemical enhancement mechanism

Nanomaterial	Raman molecule	EF	Ref.
TiN	R6G	1.0×10^5	117
VO_2	R6G	6.7×10^7	118
d-MoN	R6G	8.16×10^6	119
TiO_2nanoparticles	4-MBA	1×10^2	113
MoO_2	R6G	3.75×10^6	120
h-MoO_3	MB	6.99×10^5	121
ZnO nanocrystal	4-MPy	10^3	122
CuO nanocrystal	4-MPy	10^2	123
Amorphous Rh_3S_6	4-NBT	3×10^4	124
Amorphous ZnO nanocages	4-MBA	6.62×10^5	125
Amorphous TiO_2nanosheets	4-MBA	1.86×10^6	126
CdS nanoparticles	4-MPy	10^2	127
N-Doped graphite	CV	3.2×10^7	128
Ozone-treated graphene	RhB	2.5×10^4	129
Black TiO_2	R6G	1.2×10^6	112
$MoS_{2x}O_x$	R6G	1.4×10^5	62
WO_3	4MBA	10	130
ZnO_{1-x}	R6G	1.1×10^4	131
WO_{3-x}	R6G	1.1×10^4	131
Ga-doped ZnO nanoparticles	4-MPy	6.66×10^4	132

Published on 19 September 2022. Downloaded on 2026-01-07 6:31:26 nm..

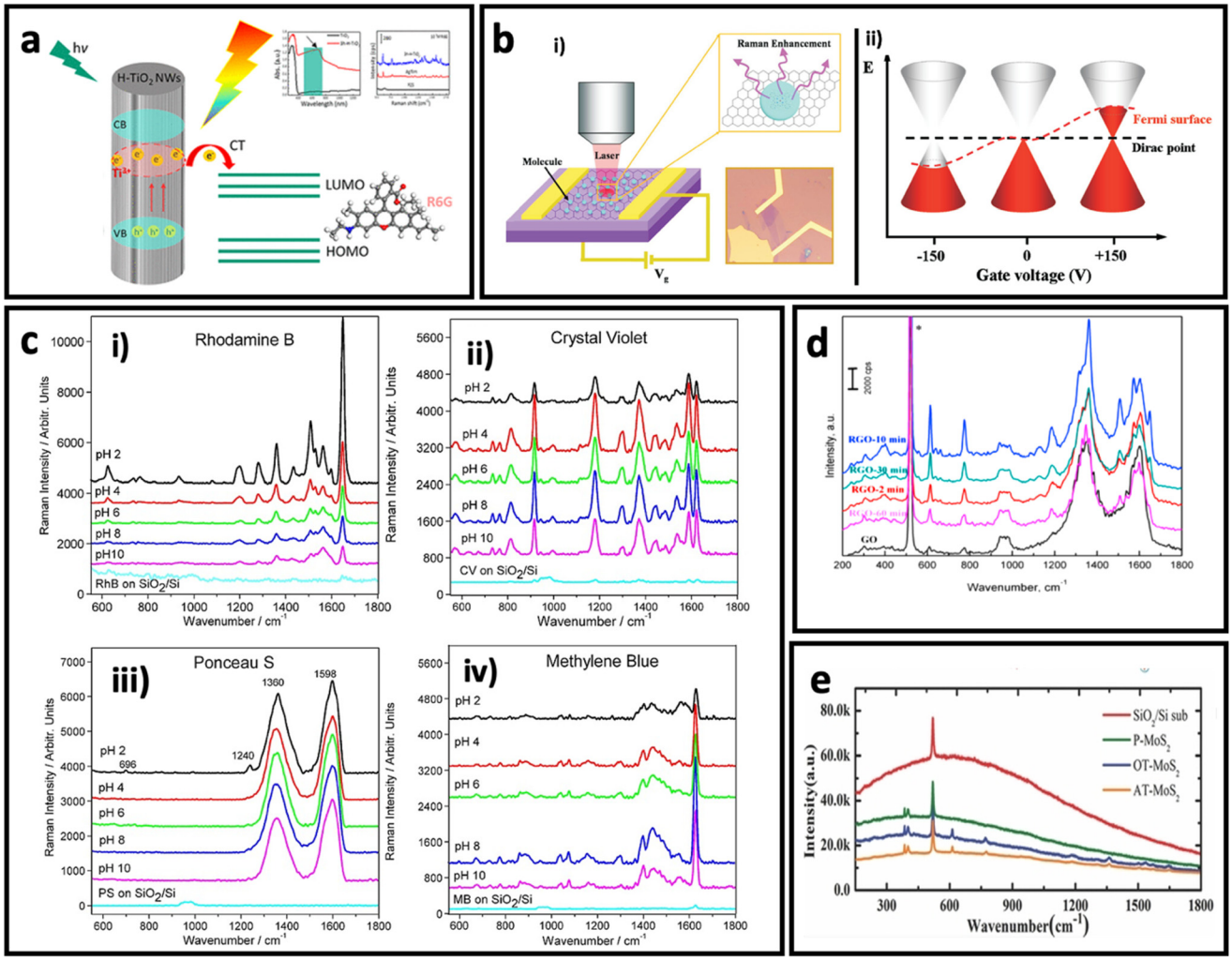

Fig. 6 (a) Schematic illustration of charge transfer process in hydrogenated TiO_2 nanowires to rhodamine 6G and its effect on SERS intensity of rhodamine 6G. Adapted from ref. 112 with permission from the American Chemical Society, copyright 2018. (b). Optical image of graphene and schematic illustration the setup (i), and effect of electrical field on Fermi level in a monolayer graphene (ii). Adapted from ref. 147 with permission from the American Chemical Society copyright 2011. (c) Effect of pH on SERS intensity of rhodamine B, 20 μM (i), crystal violet, 10 μM (ii), Ponceau S, 20 μM (iii), and methylene blue, 10 μM (iv). Adapted from ref. 161 with permission from WILEY-VCH Verlag GmbH & Co. KGaA, Weinheim, copyright 2013. (d) Effect of reduction time on SERS effect of reduced graphene oxide. Adapted from ref. 150 with permission from Elsevier, copyright 2016. (e) Raman spectra of R6G dye on different substrates: argon-plasma treated MoS_2 (AT-MoS_2), oxygen-plasma treated MoS_2 (OT-MoS_2), pristine MoS_2 (P-MoS_2), and SiO_2/Si, adapted from ref. 160 with permission from WILEY-VCH Verlag GmbH & Co. KGaA, Weinheim, copyright 2014.

treating MoO_2 with 6 wt% Li. The as-synthesized MoO_{2-x} showed better SERS performance compared with MoO_2, which could be attributed to the produced oxygen vacancies on the surface of the semiconductor, confirmed by X-ray photoelectron spectroscopy.

3.2.2. Carbon nanostructures. Carbon nanostructures, and in particular graphene-based nanostructures, have been extensively studied as SERS nanomaterials through the chemical enhancement mechanism.[142,143] Graphene has large surface area and high potential for adsorption of various molecules on its surface.[144] The quenching effect of graphene that reduces the fluorescence background in SERS measurement is another advantage.[145] Ling *et al.*[146] reported the SERS effect in graphene for the first time in 2009. They deposited graphene layers on SiO_2/Si substrate and then studied its effect on different adsorbed molecules including rhodamine 6G (R6G), phthalocyanine (Pc), crystal violet (CV), and protoporphyin IX (PPP). They found that graphene can enhance the Raman signals of all the studied molecules due to charge-transfer from graphene to the adsorbed molecules. Interestingly, they found that a monolayer of graphene leads to a stronger SERS effect. Xu *et al.*[147] have investigated the effect of the Fermi level of graphene on its SERS effect by applying positive gate voltage and negative gate voltage. They reported that the SERS effect is stronger when the Fermi level is down-shifted (*i.e.*, applying negative gate voltage) (Fig. 6b). In another work, the same group investigated the effect of an external electric field on the SERS effect of graphene under different atmospheres

 This journal is © The Royal Society of Chemistry 2022

Published on 19 September 2022. Downloaded on 2026-01-07 6:31:26 nm..

including ambient air, O_2 atmosphere, NH_3 atmosphere, and vacuum. It was found that modulation of the Fermi level region occurs differently under different atmospheres, confirming that the SERS effect in graphene comes from a charge-transfer enhancement mechanism (*i.e.*, chemical enhancement).[148] Additionally, it was found that the molecular orientation of the adsorbed molecule (*i.e.*, induced by annealing) can modulate the degree of interaction, and in turn, charge transfer between the graphene and the adsorbed molecules.[149]

Besides the graphene, the derivatives of graphene such as graphene oxide (GO) and reduced-graphene oxide (rGO) have also shown the SERS effect *via* the chemical enhancement mechanism. GO and rGO have high affinity to adsorb molecules with aromatic rings, good water dispersibility, and fluorescence-quenching capability, making them interesting candidates for SERS study. Since the pH determines the adsorption of organic molecules on the surface of GO *via* electrostatic interactions, a pH-dependent SERS effect has been observed for various molecules on GO (Fig. 6c). In rGO, Yin *et al.*[150] found that the degree of reduction can determine the SERS effect. Fig. 6d shows that rGO has a better SERS effect compared with graphene, and 10 min reduction time results in maximum SERS effect when R6G molecules are adsorbed on surface of rGO.

3.2.3. Other 2D nanomaterials. Transition metal dichalcogenides with the formula of MX_2(M is a transition metal element and X is a chalcogen element) have also shown SERS effects. Their tunable thickness, phase structure, and interlayer gap result in various photoelectric features including SERS. MoS_2, NbS_2, ReS_2, WTe_2, and $WSe_2$are some of the well-known transition metal dichalcogenides that have shown the SERS effect.[151–157] Ling *et al.*[158] investigated the potential SERS effect of MoS_2 and hexagonal boron nitride (h-BN) using copper phthalocyanine, and found that although both these nanomaterials have a weaker SERS effect compared with graphene, h-BN has better performance than MoS_2. Lee *et al.*[159] studied the effect of the number of layers of MoS_2 and WS_2 on their SERS enhancement using R6G. It was found that WS_2 has better performance than MoS_2, and in general, the increase in the number of layers decreases the SERS effect, where the change in SERS effect was pseudo-linear in MoS_2 but it decreased dramatically in WS_2. Sun *et al.*[160] reported how the treatment of MoS_2 nanoflakes can improve its SERS effect, where argon-plasma treated MoS_2 (AT-MoS_2) and oxygen-plasma treated MoS_2 (OT-MoS_2) were compared with pristine MoS2 (P-MoS_2). As can be seen in Fig. 6e, the Raman intensity of R6G is at least one order higher when it interacts with either oxygen or argon-treated MoS_2 nanoflakes.

3.3. Nanomaterials for plasmon/chemical enhancement synergic effect

In order to take advantage of both plasmon-enhancement effect and chemical enhancement effect, plasmonic nanomaterials are being combined with non-plasmonic nanomaterials (*i.e.*, semiconductors, 2D nanomaterials, *etc.*) and are being used to prepare SERS substrates. This combination not only provides higher SERS enhancement through coupling the plasmon-enhancement and chemical enhancement mechanisms, but also protects the metallic part (in particular silver) from oxidation. For example, graphene and other 2D nanomaterials have extensively been used to develop AgNP/graphene-based SERS substrates to obtain high-performance SERS systems.[162–165] The coupling between these two mechanisms can enhance the SERS effect through different pathways:[60] (i) the metal nanostructure and semiconductor each plays its own role in the enhancement of the Raman signal through the plasmon-enhancement mechanism and chemical

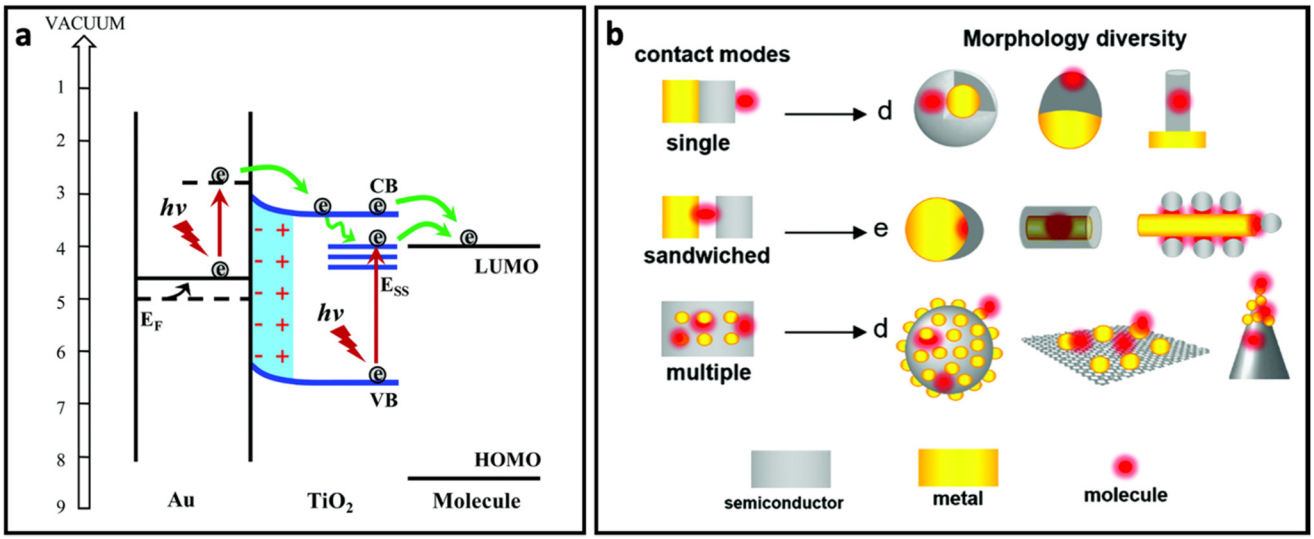

Fig. 7 (a) The role of noble metal (Au) in pumping electrons to semiconductor (TiO_2) and enhanced charge transfer from semiconductor to molecule, adapted from ref. 65 with permission from the Royal Society of Chemistry, copyright 2017. (b) Different contact modes for heterostructures containing metal (yellow), molecule (red) and semiconductor (grey) and morphology diversity for each contact mode, adapted from ref. 60 with permission from the Royal Society of Chemistry, copyright 2021.

Published on 19 September 2022. Downloaded on 2026-01-07 6:31:26 nm..

enhancement mechanism, respectively; (ii) the charge transfer rate increases due to the enhanced excitation rate in the semiconductor nanomaterial as a result of the enhanced electric field in the surrounding environment; (iii) the charge transfer rate in the semiconductor increases due to pumping electrons from noble metal to semiconductor (Fig. 7a); and (iv) distribution of the enhanced electric field can be changed and affect the Raman intensity of the adsorbed molecules. In particular, it has been reported that the enhanced electric field in between the metal islands which is usually maximum between the metal islands will shift to the surface of the metal islands in the presence of monolayered graphene. Additionally, the enhanced electric field region can penetrate into the graphene layer.[166] In addition to the better SERS performance, the metal–semiconductor-based substrates possess reproducibility owing to the self-cleaning property that comes from the improved photoinduced catalytic properties of hybrid nanostructures. All of these properties suggest that the hybrid nanostructure is favourable for designing SERS substrates. Fig. 7b represents how metal, semiconductor and molecule could be in contact with each other in different SERS system designs.[60]

4. SERS analysis of biomarkers on cells and EVs

Traditional cancer diagnostics methods involve tissue biopsy, histopathological studies and imaging (with endoscope, MRI and others). Early detection of cancer is problematic due to the limited availability of clinical assessments for the general public.[167] For most types of cancer, the above traditional diagnostics techniques are invasive and require the involvement of qualified professionals and expensive machinery, which makes cancer screening less available for patients. The limited availability of cancer screening leads to late diagnosis.[168,169] As well as availability, in most cases these techniques are able to identify potentially dangerous tumours only when the number of tumour cells is large enough to cause an extensive release of biomarkers or metastasis has started.[170]

As an analytical technique, SERS is a powerful tool for ultrasensitive analysis of small amounts of analyte, making it stand out among other techniques that require a larger amount of sample for biomarker detection. From this perspective, SERS can detect a single molecule at the designed condition.[171] SERS-based techniques have been extensively used for the detection and discrimination of biomarkers.[172–178] As discussed in sections 2 and 3 about the SERS enhancement mechanisms and substrates (nanomaterials), SERS is capable of providing a unique spectral profile for molecules on the SERS substrate – so-called "molecular fingerprints".[31,179] Additionally, the detection of cancer biomarkers with SERS is not invasive, which lowers the risk for patients and eases the analysis performance.[180–182]

Using the as-discussed SERS nanomaterials, the SERS-based analysis and detection of biomarkers on cancer cells and small extracellular vehicles (EVs) or exosomes can be classified into two main approaches: label-aided and label-free.[76]

Label-aided SERS analysis is an indirect sensing of the analyte based on the use of SERS tags, which consist of SERS-active nanoparticles functionalized with Raman-active or chromophore-based dyes that produce high-intensity and unique spectral bands/peaks. Most common label-aided detection methods utilise SERS tags that are bio-conjugated with targeting ligands, such as antibodies, to specifically target the analyte. This approach selectively identifies the target by monitoring the Raman spectrum from the SERS tag.[183] Due to the high sensitivity of this method, label-aided SERS platforms have been widely utilised in the detection of biomarkers on cancer cells and EVs.[15,16,184–187]

Label-free SERS detects the intrinsic Raman spectrum of the analyte. This method allows for the identification of molecular fingerprint signals that originate from the biomolecules in close proximity to the SERS platform (*i.e.* from the surface of the cells or EVs). This approach is simple and easy to operate, and can provide information about analytes that are difficult to differentiate by targeting a specific biomarker.[188,189] However, due to the complexity of biological systems, label-free SERS normally generates signals from all the molecules (known or unknown biomarkers) around the SERS substrate, as well as other molecules in the environment.[188] Thus, multi-variant statistical analysis methods are usually required to enable the identification of target biomarkers on cells and EVs.

In this section we discuss recent advances in SERS platform designs with plasmon and chemical enhancement effects for the analysis of cells and EVs based on two major approaches: label-aided and label-free SERS.

4.1. Label-aided SERS

There are a large variety of SERS tags with different chemical and structural properties reported in the literature.[183,189] Typically, the SERS tags' design would include nanoparticles either metallic or non-metallic NPs as the core, coated with the Raman reporter molecule (which serves as label) and targeting molecules (Fig. 8).[183,189–191] The rest of the design aims for high signal ratios to enable lower detection limits and specific targeting for reliable analysis and reproducible results. Development of label-SERS systems requires the conjugation of Raman reporter molecules to the surface of metal nanoparticles. Fig. 9 represents the chemical structure and corresponding Raman spectra of the molecules that are usually used as label or reporter in designing SERS nanotags. These molecules can be chemically attached to the surface of metal nanoparticles through strong metal–S bonds (in those that have the SH group). Metal NP@molecule (SERS nanotag) can be simply achieved by incubation of the metal nanoparticles with a solution of molecules. In order to enhance the selectivity of SERS nanotags, they can be further functionalized with various recognition elements (*i.e.*, antibody, aptamer, DNA, lectins, *etc.*) for selective targeting of the analyte. One of the most common approaches for the functionalization of metal nanoparticles is

 This journal is © The Royal Society of Chemistry 2022

Published on 19 September 2022. Downloaded on 2026-01-07 6:31:26 nm..

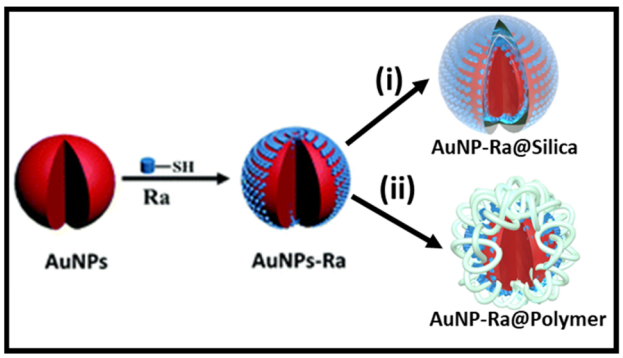

Fig. 8 Different strategies for improving the stability of SERS nanotags in biological media. Adapted from ref.193 and 197 with permission from Elsevier, copyright 2019, and the Royal Society of Chemistry, copyright 2020, respectively.

using linkers that can bind to metal nanoparticles from one head and provide functional groups such as COOH and NH_3 on their other head. The COOH or NH_3 groups can be further linked to recognition elements through *N*-hydroxysuccinimide (NHS)/*N*′-ethylcarbodiimide hydrochloride (EDC) chemistry.[192] Another approach is using a linker that can directly be attached to a recognition element. For example, we have reported the functionalization of AuNPs with lectins (*i.e.*, WGA, cholera toxin B (CTB), *Phaseolus vulgaris* (PHA-L) and *Aleuria aurantia* lectin (AAL)) using (3,3′-dithiobis (sulfosuccinimidyl propionate)) (DTSSP) as linker. In this approach, lectin-DTSSPs were first incubated with 1 : 1 mass ratio and the obtained complexes were incubated with AuNPs.[193] Besides covalent functionalization, electrostatic interaction between the recognition element and metal nanoparticles covered by molecules is another approach. However, since this electrostatic interaction is loose, there is the need to consider the stability of the binding for biomedical applications. While the SERS nanotags are of great importance for *in vitro* and *in vivo* applications, their stability in the biological environment is one of the main concerns. To address this drawback, there are two main approaches: (i) formation of a silica shell to protect the metal core from oxidation (*i.e.*, in the case of silver) and increase the colloidal stability; and (ii) coating with macromolecules (*i.e.*, polymers, proteins, *etc.*) (Fig. 8). In a comparative study, we found that a layer of bovine serum albumin (BSA) on the SERS nanotag could result in more stability in

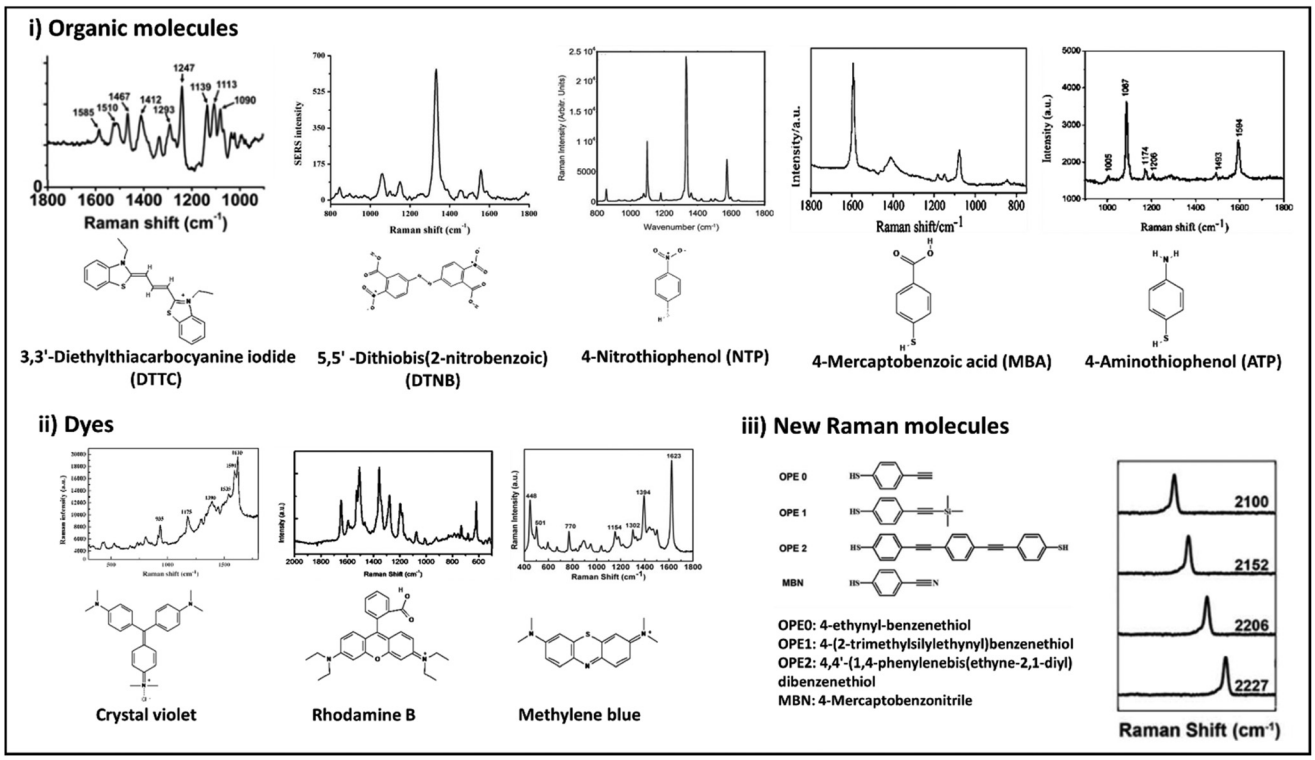

Fig. 9 Chemical structures and Raman spectra of different Raman molecules including small organic molecules (i), dyes (ii), and newly designed Raman molecules (iii). DTTC: adapted from ref. 198 with permission from the American Chemical Society, copyright 2021. DTNB: adapted from ref. 199 with permission from Nature-Springer Group, copyright 2018. NTP: adapted from ref. 200 with permission from WILEY-VCH Verlag GmbH & Co. KGaA, Weinheim, copyright 2020. MBA: adapted from ref. 201 with permission from the American Chemical Society, copyright 2016. ATP: adapted from ref. 202 with permission from the Royal Society of Chemistry, copyright 2012. Crystal violet: adapted from ref. 203 with permission from Elsevier, copyright 2012. Rhodamine B: adapted from ref. 204 with permission from Nature-Springer Group, copyright 2015. Methylene blue: adapted from ref. 205 with permission from Elsevier, copyright 2016. New Raman molecules: adapted from ref. 206 with permission from the American Chemical Society, copyright 2018.

Published on 19 September 2022. Downloaded on 2026-01-07 6:31:26 nm..

biological media (*i.e.*, 1X PBS, 1 M Tris-HCl, FPBS and RF-10) than the formation of a thin layer of silica. However, it was found that the stability of the antibody-functionalized BSA-coated SERS nanotags strongly depends on the type of antibody and also the thickness of this extra layer. Therefore, the stability of SERS nanotags should be investigated in each case. As discussed in previous sections, the nanoparticles that serve as the core for the SERS tag can provide plasmonic or non-plasmonic Raman signal enhancement as well as enabling hybrid SERS. The nature of the phenomenon depends on the chemistry of the core. In case of plasmonic label-aided SERS, nanoparticles are manufactured from noble metals like gold or silver.[194,195] For the non-plasmonic label-aided SERS, the core of SERS tag can be any material that provides chemical Raman signal enhancement, such as semiconductors, carbon nanostructures and transition metals.[178,196] In this section we discuss recent advances in label-aided SERS platforms that incorporate described SERS tags designs based on the plasmonic and chemical/hybrid enhancement of Raman signal.

4.1.1. Plasmon enhancement platforms. Owing to the high SERS enhancement factor, most SERS nanotags or label-aided SERS detection have used plasmonic nanoparticles. Numerous published works focus on developing SERS platforms that can provide high sensitivity, enabling up to femto molar analyte concentration detection. Researchers are coming up with new SERS platform design variations, observing plasmon enhancement originating from multiple hotspots on anisotropic particles created by local curvature and hotspots formed by cavities between noble metals (core–shell structures, nanohollows).[207–210] A good example of such design is reported by Fan *et al.*,[211] who developed a SERS sensor for ultrasensitive exosome (isolated from A549 cell medium) detection using Au nanostars as substrate and Raman reporter (4-MBA) coupled with lysine as SERS tags and targeting molecule, respectively (Fig. 10a). This platform allows optimization of signal amplification, due to the controlled coupling of the Raman reporter with lysine by solid-phase peptide synthesis. The authors have reported ultrasensitive exosome quantification with the limit of detection of 2.4 particles per μL.[211]

An interesting approach was developed to increase the detection sensitivity of EVs in which they are labelled with SERS tags conjugated with capturing substrates, enabling separation and accumulation of the analyte into a small area for ultrasensitive detection.[184,212,213] This approach also eliminates the need for complex analyte isolation procedures from biological media. As indicated in Fig. 10b, Hou *et al.* developed a dual aptamer-based sandwich-type SERS sensor for quantitative detection of tumour-derived EVs.[212] The EVs were

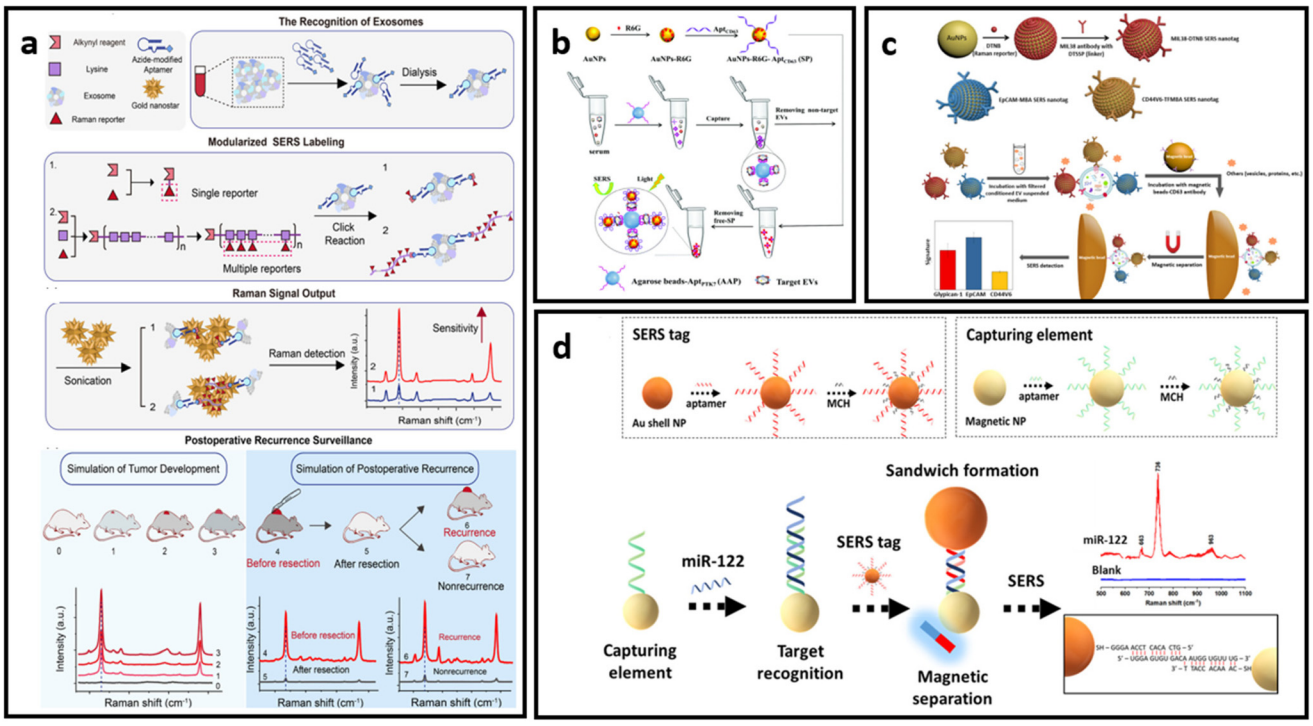

Fig. 10 (a) Protocol of ultrasensitive exosome detection *via* SERS biosensor based on Au nanostars as substrate and Raman reporter coupled with lysine as SERS tags and targeting molecule, respectively; adapted from ref. 211 with permission from the American Chemical Society, copyright 2021; (b) sandwich-type SERS sensor based on dual aptamers and Au-enhanced Raman signal probes for the detection of tumour EVs; adapted from ref. 212 with permission from the Royal Society of Chemistry, copyright 2020; (c) detection of multiple cancer-specific surface proteins on EVs (molecular phenotype profiling) of CD63-positive EVs using SERS nanotags and CD63 antibody-functionalized magnetic beads; adapted from ref. 184 with permission from the American Chemical Society, copyright 2020. (d) Aptamer functionalized SERS-sandwich assay for ultrasensitive detection of miR-122 from exosomes, adapted from ref. 213 with permission from the American Chemical Society, copyright 2021.

This journal is © The Royal Society of Chemistry 2022

Published on 19 September 2022. Downloaded on 2026-01-07 6:31:26 nm..

immobilized on the surface of agarose beads functionalized with aptamers targeting PTK7 (tyrosine kinase-7) proteins, which are highly expressed in tumour-derived exosomes. Captured EVs were then labelled with SERS tags that consist of AuNPs decorated with R6G and aptamers targeting CD63 proteins which are pervasively expressed on targeted EVs. The concentrated precipitate could then be analysed *via* SERS. Another example of this approach was implemented by Zhang *et al.*, where CD63-modified magnetic beads were used as capturing substrates.[184] EVs immobilised on the magnetic beads were labelled with three different SERS tags – AuNP decorated with Raman reporter molecules (DTNB, MBA or TFMBA) and conjugated with monoclonal antibodies for specific binding (CD44V6, EpCAM and MIL38) (Fig. 10c). This approach enabled the simultaneous detection of multiple cancer-specific surface proteins on EVs in a single sample. As a proof-of-concept demonstration, their method was further tested in plasma-derived EVs in patients who have experienced PDAC.[178] The magnetic separation method is suitable not only for EV detection, but can be implemented to concentrate and separate the EVs' and exosomes' protein biomarkers of interest, as has been done by Muhammad *et al.*[213] The researchers developed an aptamer SERS-sandwich assay for highly sensitive detection of elevated exosomal miR-122. The biosensor was constructed with a SERS tag (silica-coated AuNP conjugated with aptamer and Raman reporter molecule) and magnetic capture substrate (Au-coated Fe_3O_4 NP functionalised with the target-recognition aptamer) (Fig. 10d). The researchers demonstrated that separated exosomal miR-122 can be recognized with the coexistence of other sequences of similar length with a slightly varying arrangement of DNA bases in a concentration as low as 8 fM.[213]

Label-aided SERS sensors can be integrated for multiplex and robust quantitative analysis with miniaturized devices for "at the point-of-care" testing. The conceptual design of such devices avoids the use of the complex protocols that hinder point-of-use of the developed techniques. As such, Reza *et al.*[214] developed a SERS-based simple microfluidic device for screening of single CTC that enables the identification of the heterogeneous expression of CTC surface proteins (Fig. 11a). They have employed three types of Raman reporter molecules for the SERS-tags (DTNB, MBA, and TFMBA) for each type of biomarker analysed through the channel. CTC passing through the microfluidic channel was then analysed for the heterogeneous expression of multiple cell receptor proteins. The second part of the device consists of an electrochemical zone with nanoscopic fluid mixing for the detection of intracellular protein. By enhancing the antigen–antibody collision *via* nanoscopic mixing, the sensitivity of detection is significantly increased.[214] Wang *et al.*[215] adopted a similar nanoscopic fluid-mixing chip with SERS-based nanobarcode sorting for the detection of different EVs subpopulations (Fig. 11b). They have seen the elevated sensitivity of the platform due to the created nanoscopic flow. The reported detection limit was 10^3 particles per mL.[215]

Overall, the described strategies have been developed in order to provide the most accurate analysis of CTCs or EVs in complex biological media, with a low limit of detection. A summary of the methods described above is presented in Table 2.

4.1.2. Chemical enhancement and hybrid platforms. Since the chemical enhancement mechanism is not strong enough to produce a high-intensity Raman signal, the development of SERS systems with only chemical enhancement has faced challenges. However, to increase the SERS sensitivity of the biosensor, common noble metallic nanostructures are incorporated with semiconductor materials such as TiO_2, graphene, ZnO, Cu_2O and others, as discussed in section 2 and section 3. These materials provide chemical enhancement in addition to the strong EM enhancements generated by the plasmonic NPs. The combination of the chemical and plasmon SERS platforms improves the detection limits as compared with the SERS platforms on their own, greatly benefitting sensing in low analyte concentrations. Hybrid SERS platforms combine the beneficial properties of the materials and overcome the limitations of traditional noble metal-based SERS platforms with improved reproducibility, stability and biocompatibility.[60,61] A good example of such a synergetic combination is a TiO_2@Ag nanostructure, developed by Xu *et al.* for the ultrasensitive detection of CTCs.[217] The authors prepared a TiO_2@Ag nanostructure by modifying Ag on the surface of TiO_2 NPs. The particles are further functionalised with R6G molecules (SERS tag), reduced bovine serum albumin (rBSA, increase stability and reduce non-specificity binding) and folic acid (FA, target molecule to specifically recognize cancer cells) (Fig. 12(i)). These prepared nanostructures are reported to have ultrahigh sensitivity, good specificity, low toxicity, and high accuracy in CTC detection. According to the results of the study, the TiO_2@Ag nanostructure demonstrate SERS activity with an EF of up to 7.61×10^7 (lower limit of detection for R6G is 10 fM). The developed TiO_2@Ag–R6G–rBSA–FA SERS bioprobe was effectively utilized in detecting various cancer cells in samples with rabbit blood and clinical liver cancer blood samples (Fig. 12(ii–v)). The sensitivity of the bioprobe towards CTC was 1 cell per mL.[217]

Semiconductor materials provide another beneficial feature: photothermal (PT) conversion. The combination of SERS properties and local PT effects gives SERS platforms additional functionality as theranostic agents – targeting, detection/sensing and photothermal destruction of tumour cells. Hybrid SERS platforms with PT conversion provide sufficient EM signal enhancement for imaging and probe sensing.[218–222] Semiconductor materials are also able to provide a strong SERS signal and PT effect without incorporation of Au.[223,224] Lin *et al.* reported ultrahigh SERS activity (EF up to 10^5 for the nitro blue tetrazolium (NBT) probe molecule) of crystal–amorphous core–shell-structured black-TiO_2 NPs.[225] The designed core–shell structure enables high-efficiency exciton transition resulting in charge-separation that occurs due to interfacial band bending. Those effects induce photo exciton transition from the crystal core to the amorphous shell, further promoting photoinduced charge transfer between the substrate and probe molecule. Modified with SERS-active molecule (tag) and antibody (targeting molecule),

Published on 19 September 2022. Downloaded on 2026-01-07 6:31:26 nm..

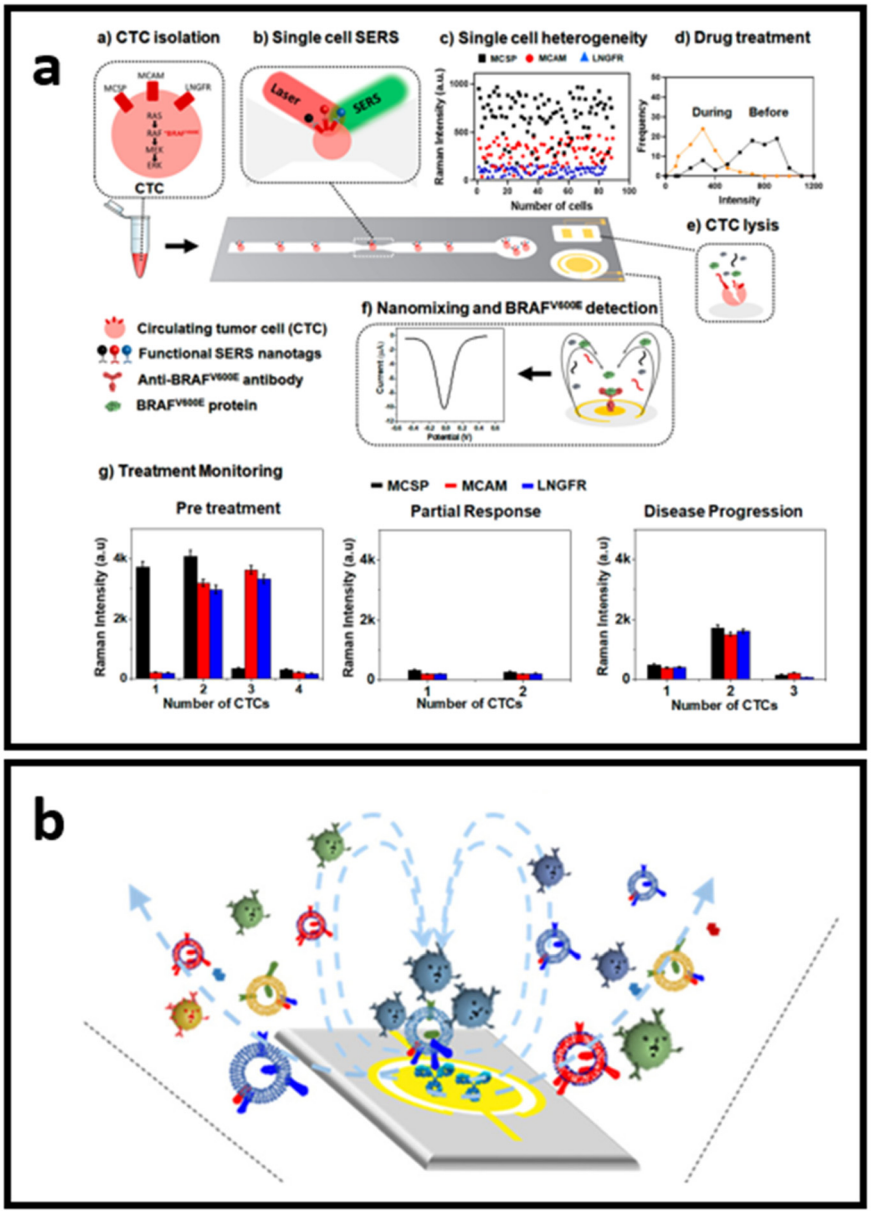

Fig. 11 Schematics of the small devices with SERS-based sensors: (a) SERS-based microfluidic immunoassay for *in situ* characterization of single CTCs, adapted from ref. 214 with permission from the American Chemical Society, copyright 2021; (b) nano-mixing-enhanced EVs subpopulation characterization platform adapted from ref. 215 with permission from the American Chemical Society, copyright 2021.

the core–shell-structured TiO_2 NPs can be used to quickly and accurately identify cancer cells in order to efficiently administer treatment with photothermal therapy.[225] Hybrid SERS platforms are often used to incorporate additional chemical enhancements that increase overall SERS sensitivity. However, a typical constraint of such an approach is that chemical or physical binding of the analyte is required to produce effective chemical enhancement through charge transfer, limiting the choice as it requires the analyte to have either a thiol or aromatic binding group. Further, there are limited reports on the usage of hybrid systems to improve SERS through EM, which is a long path for development. Unfortunately, employing a particular linker to detect and identify disease-related CTC and EVs is rather difficult. The complex nature of cells and EVs including many biomolecules makes it difficult to identify particular biomarkers for selective labelling.[226,227] As a result, identifying possible disease-related cells or EVs requires a more thorough strategy that takes into account signals from both known and undiscovered biomarkers to distinguish individuals at risk from healthy donors.

4.2. Label-free SERS

It is very important to understand that successful data analysis with a label-free SERS platform depends on both a strong,

 This journal is © The Royal Society of Chemistry 2022

Published on 19 September 2022. Downloaded on 2026-01-07 6:31:26 nm..

Table 2 Recent advances in ultrasensitive detection of various biomarkers on cells and EVs using plasmon-enhanced SERS system

SERS platform	Biomarkers	Media	Described detection ability	Ref.
Au–Ag nanohollows	T24 and RT4 bladder cancer cells	Urine	Detection limit up to 1250 cells	209
Porous $CuFeSe_2$/Au heterostructured nanospheres	Gaseous aldehydes and lung cancer cells (A549)	Exhaled breath and cultured cells	Detection limit of gaseous aldehydes – 1.0 ppb; detection of folate receptor-positive cancer cells	210
AuAg NPs SERS tags with Fe_3O_4@TiO_2 capturing substrate	EVs derived from A549 and normal human bronchial epithelial (BEAS-2B) cells	Human serum	Detection limit 1 particle per mL	216
AuNPs SERS tags with agarose beads capturing substrate	EVs derived from human acute lymphoblastic leukemia cells (CCRF-CEM)	Human serum	Detection limit 2.44 pg μL^{-1}	212
AuNPs SERS tags with magnetic beads capturing substrate	EVs derived from colorectal cancer (SW480), bladder cancer (C3) and pancreatic cancer (Panc-1)	Human serum	Phenotype profiling with low sample volume – 10 μL	184
AuNPs SERS tags with Fe_3O_4@TiO_2 capturing substrate	miRNA inside EVs derived from Panc-1 cells	Human serum	*In situ* analysis with detection limit of 0.21 fM	186
SERS EpCAM-aptasensors	EVs derived from A549	Isolated exosomes (cell medium of A549 cells)	Detection limit 2.4 particles per μL	211
SERS-based microfluidic immunoassay for *in situ* characterization of single CTCs	CTCs from melanoma cells (SK-MEL-28)	Isolated cells (patient's sample)	Single cell-level protein expression profiling	214
Aptamer functionalized SERS-sandwich assay	miR-122 from mice serum and human hepatoma (HepG2) cells' EVs	Isolated EVs (mice serum and cell medium of HepG2 cells)	Detection limit 8 fM	213
Nano-mixing-enhanced subpopulation characterization platform	EVs derived from SK-MEL-28, SK-MES-1, NCI-H1703, NCI-H1650, and MCF7 cells	Isolated EVs (SK-MEL-28, SK-MES-1, NCI-H1703, NCI-H1650, and MCF7 cells culture media or plasma)	Detection limit 10^3 particles per mL	215

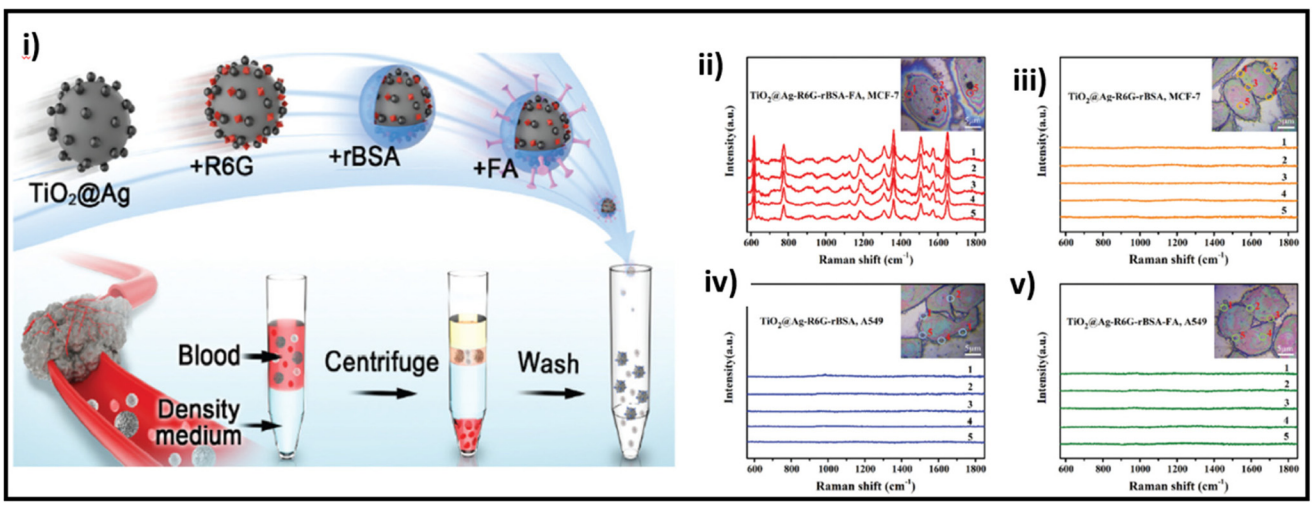

Fig. 12 (i) Schematic of the preparation of TiO_2@Ag-based SERS bioprobe; SERS detection of MCF-7 and A549 cells incubated with TiO_2@Ag–R6G–rBSA–FA (ii and v, respectively) and TiO_2@Ag–R6G–rBSA (iii and iv, respectively) SERS bioprobes. Adapted from ref. 217 with permission from the Royal Society of Chemistry, copyright 2022.

reliable and accurate Raman signal, of which the SERS substrate is in charge, and analysis of the signal. The Raman data acquired by the label-free SERS method contain huge amounts of information, especially when the analyte consists of multiple biomolecules that provide a complex pattern of signature peaks. The most common approach to interpreting SERS signals is to examine particular Raman bands attributed to the known vibrational modes and analyse the discernible differences in intensity and Raman shift compared with the control samples. Bioanalytes, such as proteins, nucleic acids and lipids, are usually analysed based on the spectral fingerprint areas (between 800 and 1800 cm^{-1}) (Fig. 13).[228] However, it is

Published on 19 September 2022. Downloaded on 2026-01-07 6:31:26 nm..

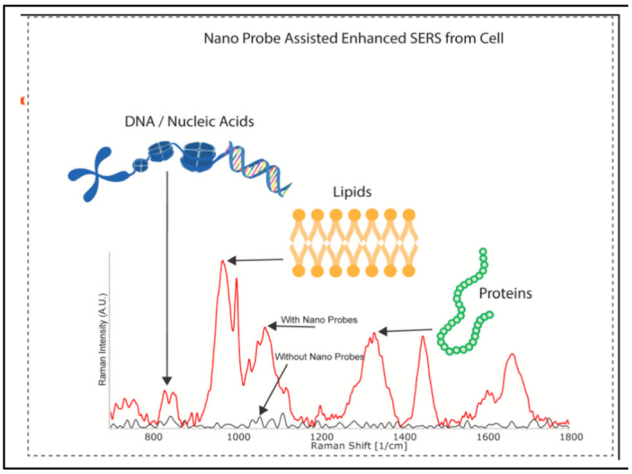

Fig. 13 Characteristic Raman peaks of biomolecules, adapted from ref. 228 with permission from Elsevier, copyright 2021.

difficult to clearly identify the difference in signals from cells and EVs due to the interference from various substances. Therefore, to use the SERS signal of more complex structures as a fingerprint for disease diagnosis, more precise signal analysis methods are used such as multivariate statistical methods (principal component analysis, "PCA"),[229–232] and the more recently developed methods of machine learning[231,233] and neural networks.[234,235] We will not discuss much about analysis techniques, focusing on the SERS platforms themselves, but the reader should take into consideration that label-free SERS analysis outcome depends 50% on data analysis tools.

Label-free SERS analysis is attractive to scientists due to the rich information outcome it provides. Apart from the importance of data analysis that we briefly mentioned, the direct SERS approach suffers multiple drawbacks that researchers are willing to tackle through the SERS platform designed to harvest the major benefit of analytes' full structural information. In this section, we discuss the label-free SERS approach with the aim to deliver the advances in plasmon and chemical/hybrid enhancement approaches in the design of sensing platforms for the analysis of cells and EVs.

4.2.1. Plasmon enhancement platforms. Obtaining a strong, clear and reproducible Raman spectrum is very important in label-free SERS analysis. The final spectral profile of the analyte depends on many factors related to the SERS platform, such as the optical properties of the plasmonic material, laser excitation wavelength, Raman cross-section of the target analyte, analyte surface coverage and localization. Typically, biological molecules produce extremely low signal intensities. Due to the distance-dependent nature of the SERS effect, as discussed in section 2.1, the local electric field enhancement rapidly decreases with the increase in the distance from the metal surface. To overcome these problems related to low intensities and the heterogeneous nature of the cells' and EVs' Raman signals, researchers have developed methods to place analytes in SERS hotspots. These methods aim to design an effective capturing substrate that would create signal enhancement in the place of analyte capture. An example of such a consideration in a label-free SERS platform was demonstrated by Liu *et al.*,[232] who utilized anisotropic Au–Ag nanostars that provide multiple "hot-spots" to distinguish the spectral differences of pancreatic cancer EVs from different sources (Fig. 14a). Positively charged Au–Ag nanostars were attracted to negatively charged EVs *via* electrostatic forces, resulting in SERS spectra showing characteristic Raman peaks of the different components of the EVs. The detection limit of comprehensive analysis was 6.7×10^8 EVs per mL.[232] Ćulum *et al.*[229] developed SERS substrates with Au nanohole arrays of varying sizes and shapes (Fig. 14b). These platforms have dual purposes of trapping single EVs and enhancing their vibrational signature.[229] Ren *et al.* presented the nanolaminated SERS multi-well cell culture assay (Fig. 14c). The cells can be cultured directly onto the SERS substrate, enabling 100% detection. The platform integrates a multi-layered "metal–insulator–metal" nanolaminated SERS substrate and polydimethylsiloxane (PDMS) multi-wells for simultaneous analysis of the cultured cells. With the aid of this platform and machine learning, the authors managed to distinguish, with an accuracy close to 90%, the border where breast cancer cell lines end and normal breast epithelial cells begin. The prediction rate between breast cancer cells and prostate cancer cells was 94%.[236] An alternative to promote EVs–NPs interactions is described in the work of Fraire *et al.*[231] These researchers developed a label-free SERS analysis of EVs based on *in situ* formation of core–shell NP Au@Ag NPs directly on the EV surface. AuNPs were modified with 4-(dimethylamino)pyridine (DMAP) to impart positive charge and electrostatically adhere onto EVs. To ensure a reliable SERS signal, capping agent (DMAP) spectral contributions were quenched further by an *in situ*-grown Ag layer (Fig. 14d). Additionally, core–shell NP Au@Ag boosts EVs' Raman signal.

Most reports demonstrate that label-free SERS necessitates the use of pre-treated samples to avoid signal detection from other molecules in the surrounding medium that are unrelated to the analyte. Indeed, the purity of the sample is critical, as it affects the reliability and repeatability of the SERS analysis. Using a label-free SERS platform, Koster *et al.*[233] verified that common EV isolation methods (differential ultracentrifugation, density gradient ultracentrifugation, and size exclusion chromatography) yield variable lipoprotein content. For their tests, the research group developed a SERS platform based on a commercially available substrate composed of a quartz microfiber matrix embedded with AuNP clusters (solid Au spheres with an approximate diameter of 40–60 nm), grafted to a borosilicate glass microscope slide. After analysing different samples, the authors concluded that a dual-isolation method is necessary to isolate EVs from the major classes of lipoprotein for the better performance of the label-free SERS platform. The authors also reported that combined machine learning analysis and the developed SERS platform was sensitive enough to identify cancer-specific signatures that

 This journal is © The Royal Society of Chemistry 2022

Published on 19 September 2022. Downloaded on 2026-01-07 6:31:26 nm..

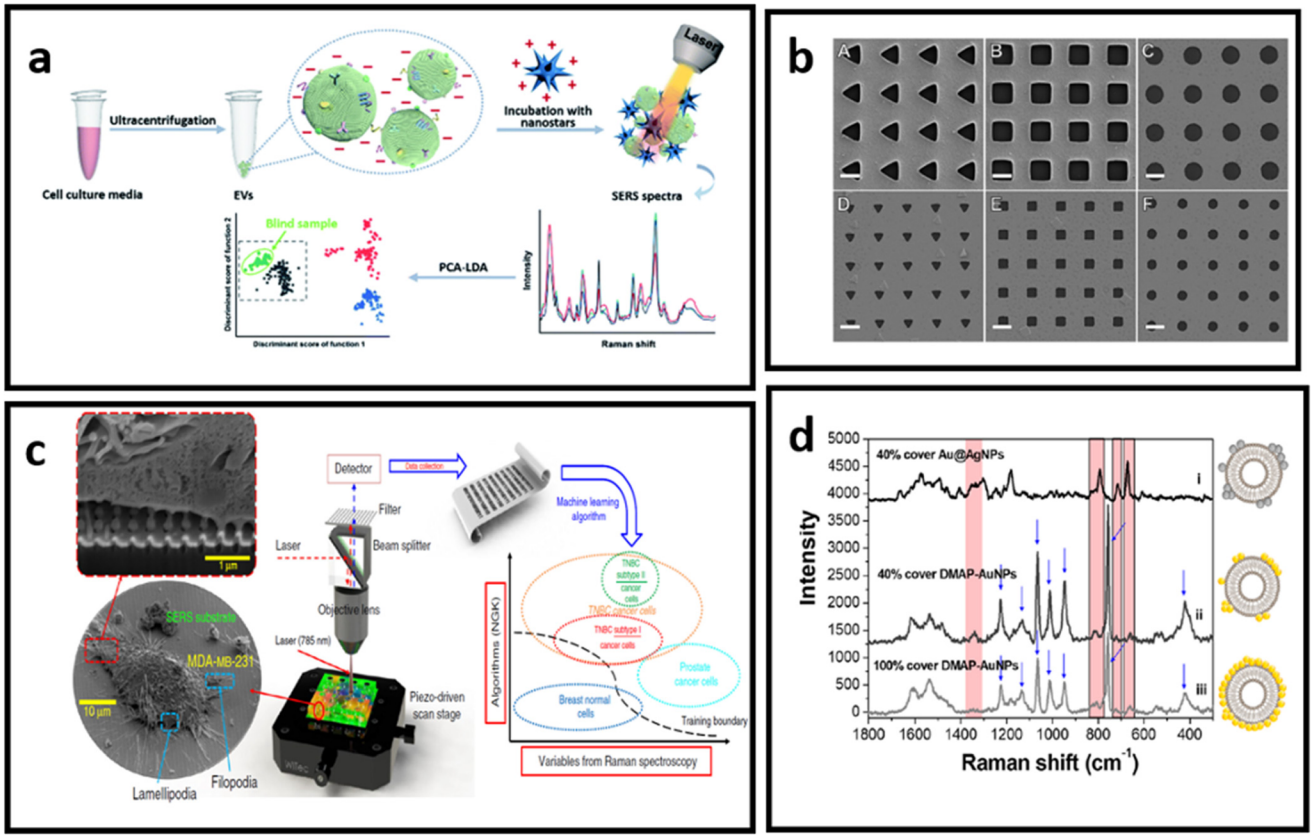

Fig. 14 (a) Molecular characterisation of EVs with positively charged gold nanostars, adapted from ref. 232 with permission from the Royal Society of Chemistry, copyright 2020; (b) Au nanohole arrays of varying sizes and shapes for trapping single EVs and enhancing their vibrational signature, adapted from ref. 229 with permission from Springer-Nature Group, copyright 2021; (c) nanolaminated SERS multiwell cell culture assay, adapted from ref. 236 with permission from Springer-Nature Group, copyright 2020; (d) *in situ* EV-attached AuNPs with a grown over silver layer – to form a core–shell nanoparticle (Au@AgNPs) directly at the EV surface, adapted from ref. 231 with permission from the American Chemical Society, copyright 2019.

remained unaffected by the presence of additional co-isolated biomolecules, showing that the label-free diagnostic ability was effective across many different sample preparations.

4.2.2. Chemical enhancement and hybrid platforms. Among chemical enhancement platforms for label-free SERS detection of biomarkers, the prevailing number is based on plate substrates. The trend is similar to that previously described – there is a need for strong, reliable and accurate Raman measurement that is achieved through increased EM enhancement.[237,238] Haldavnekar *et al.* developed a label-free SERS approach for the specific detection of biomolecules on the cells by using extremely small ZnO NPs (sub 10 nm).[228] ZnO is a wide band gap material, hence a good candidate for biomolecular sensing applications. The probes demonstrated significant SERS enhancement (EF – 10^6 with 4-ATP and 4-MBA analyte molecules). After cellular uptake, an increased nanoprobes signal was achieved for the signals of cellular components – amplification of around 7-fold for DNA, 16-fold for proteins and 24-fold for lipids (Fig. 15a).[228]

Analyte-capturing techniques are also being extensively researched and developed, as an approach to achieving strong and accurate SERS signal rests on the analyte. Yin *et al.* demonstrated a facile polyethylene glycol (PEG)-based isolation method to classify and further analyse EVS with a label-free SERS platform.[239] PEG is commonly used to bind and purify *via* centrifugation virus particles.[240] The PEG-based method was adapted to isolate EVs,[241] which were similar to viruses in physical size and membrane structure. EVs were wrapped in PEG films, and upon centrifugation formed PEG-based EV aggregates. The authors used a novel planar nanomaterial – amino molybdenum oxide (AMO) nanoflakes – as the SERS substrate.[242] To prove the reliability of the platform, three types of common male cancer cell lines – leukemia, prostate cancer, and colorectal cancer – and one healthy male blood sample, were utilized to isolate and classify EVP. The obtained data were analysed by PCA and machine learning algorithm. As a result, analysis accuracies were higher than 85% and all the precisions and sensitivities were higher than 80% for all tested cell lines.[239]

Semiconductors exhibit plasmon-free SERS through the electron transferring between the semiconductor and adsorbed analytes.[243] As such, Zhang *et al.* developed a

Published on 19 September 2022. Downloaded on 2026-01-07 6:31:26 nm..

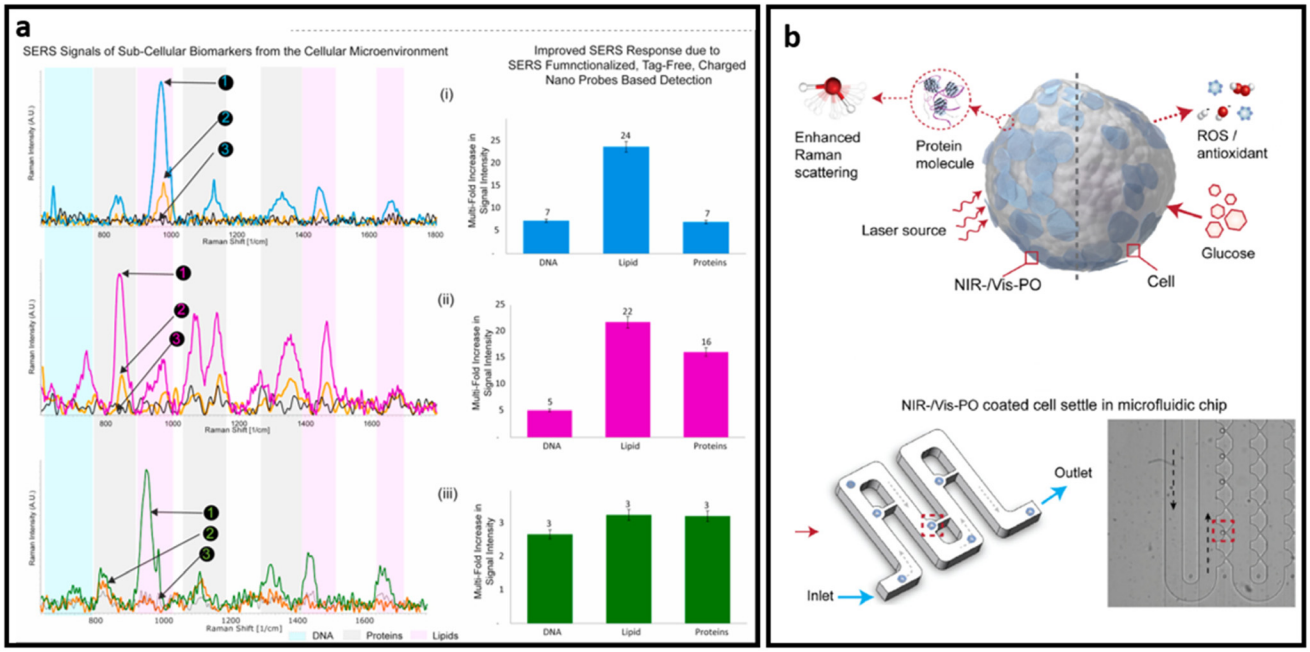

Fig. 15 (a) SERS signals of sub-cellular biomarkers in cancer cell by self-functionalized tag-free nano sensor, adapted from ref. 228 with permission from Elsevier, copyright 2021; (b) schematic SERS detection *via* PO nanoprobe: PO-coated cell SERS sensing (top) and optical image of the PO-coated cells infused into a microfluidic chip and settled separately in the small grooves, highlighted in red (bottom), adapted from ref. 243 with permission from Elsevier, copyright 2022.

dopant-driven oxide-based label-free SERS substrate with dual function. For the SERS measurement, cells were briefly (10 min) incubated with plasmonic oxide NPs. Then authors used a microfluidic chip system with grooves designed to hydrodynamically trap individual cells from the suspension and minimize possible interference on the target signals from the medium. The trapped single cells were then further analysed with a Raman spectrometer (Fig. 15b). The developed platform exhibits up to 90% accuracy in distinguishing single leukemia (THP1) cells from peripheral blood mononuclear cells (PBMC) and human fetal kidney (HEK 293) from a human macrophage cell line (U937). Based on the combined features of enhanced electromagnetic field-driven SERS and dopant-driven tunable plasmonics, this approach enables single-cell detection. In addition, the nanoprobe is triggered by the bio-redox response of individual cells to stimuli, enabling complementary colorimetric cell detection and achieving nearly uniform identification accuracy at the single cell level.[243] A stronger Raman signal in label-free design is necessary to obtain distinct peaks from various biomarkers that exist on the surface of cells and EVs, leading to better analysis of samples through profiling the most possible biomarkers on their surfaces. Given that the combination of chemical enhancement and plasmon enhancement in the design of SERS substrates provides a higher SERS enhancement factor, many semiconductors and 2D nanomaterials have been combined with noble nanostructures to make ultra-sensitive SERS substrates.[244,245]

5. Conclusions, perspectives and future directions

SERS is one of the main approaches for ultrasensitive analysis of wide ranges of analytes for biomedical purposes. Various nanomaterials, ranging from plasmonic noble metal nanostructures to inorganic semiconductors and 2D semiconductor nanosheets, have been extensively used for the mechanistic study of SERS as well as in designing SERS systems in both colloidal and planar forms. One of the main challenges in comparing the SERS efficiencies of different nanomaterials is the inconsistencies in calculation of the SERS enhancement factor, where there is a variety of parameters (such as solid sample *vs.* colloidal solution). In mechanistic studies, researchers usually ignore one of the mechanisms and attribute the observed SERS solely to one of the main well-known mechanisms. Although one of the mechanisms is usually dominant – electromagnetic enhancement is dominant in metal nanoparticles and chemical enhancement is dominant in semiconductors – a comprehensive analysis should be performed to indicate the role of each mechanism in SERS of new nanomaterials.

SERS biosensors have been designed for the analysis of various biomarkers in biological samples, and in particular, molecular signatures of cells and their extracellular vesicles. These SERS systems can be categorized into two main groups: label-aided and label-free SERS systems. Label-aided and label-free SERS present both great advantages and challenges. While the use of SERS tags allows ultra-sensitive detection of analytes and relatively simple

 This journal is © The Royal Society of Chemistry 2022

Published on 19 September 2022. Downloaded on 2026-01-07 6:31:26 nm..

manufacturing, it does not provide any structural information about the target molecules other than their presence. In addition, despite the development of SERS nanotags, there is still a need to develop SERS nanotags with high intensity and high colloidal stability in biological media, and reproducible SERS to make it more reliable in biomedical applications.

On the other hand, label-free SERS can provide structural information about the target sample. However, the analysis and interpretation of spectra from complex structures made up of many biomolecules are equally difficult, and necessitate the use of sophisticated data-processing techniques to enable reliable interpretation of complicated vibrational patterns. Although many machine learning-based techniques have been utilised to analyse the SERS spectra of complex samples, many methods still have not been investigated. Additionally, there is no comprehensive analysis comparing the accuracy of these techniques. The establishment of a standard method becomes very urgent and of significance for label-free SERS assays.

The further development of plasmonic and conductive materials would greatly benefit the SERS sensing technology, where there is a need to investigate the SERS performance of newly developed nanomaterials such as carbon dots and metal nanoclusters, and aggregation-induced emission luminogens which have shown great optical properties and, in particular, excellent charge/energy transfer ability. Additionally, the development of SERS biosensors should also move towards a more conceptual design of the platform. While most of the described techniques demonstrated reproducible and reliable results with low detection limits, the SERS platform compositions and protocols in the majority of the works are rather complicated for point-of-care use. The construction of small devices based on the powerful SERS platform, as well as reliable and powerful analysis tools, that would allow minimum effort from the user to perform analysis is one of the most important pathways for the development of this technology.

Conflicts of interest

There are no conflicts to declare.

Acknowledgements

This work was supported by the Australian Research Council (ARC) through Discovery Projects (DP200102004). A. T acknowledges funding support from the International Macquarie University Research Excellence scholarship (iMQRES).

References

1 A. Smekal, *Naturwissenschaften*, 1923, **11**, 873–875.
2 R. Singh, *Phys. Perspect.*, 2002, **4**, 399–420.
3 J. J. Laserna, *Modern techniques in Raman spectroscopy*, Wiley New York, 1996.
4 E. Smith and G. Dent, *Modern Raman spectroscopy: a practical approach*, John Wiley & Sons, 2019.
5 K. Kneipp, H. Kneipp, I. Itzkan, R. R. Dasari and M. S. Feld, *Chem. Rev.*, 1999, **99**, 2957–2976.
6 M. Fleischmann, P. J. Hendra and A. J. McQuillan, *Chem. Phys. Lett.*, 1974, **26**, 163–166.
7 J. Langer, D. Jimenez de Aberasturi, J. Aizpurua, R. A. Alvarez-Puebla, B. Auguié, J. J. Baumberg, G. C. Bazan, S. E. J. Bell, A. Boisen, A. G. Brolo, J. Choo, D. Cialla-May, V. Deckert, L. Fabris, K. Faulds, F. J. García de Abajo, R. Goodacre, D. Graham, A. J. Haes, C. L. Haynes, C. Huck, T. Itoh, M. Käll, J. Kneipp, N. A. Kotov, H. Kuang, E. C. Le Ru, H. K. Lee, J.-F. Li, X. Y. Ling, S. A. Maier, T. Mayerhöfer, M. Moskovits, K. Murakoshi, J.-M. Nam, S. Nie, Y. Ozaki, I. Pastoriza-Santos, J. Perez-Juste, J. Popp, A. Pucci, S. Reich, B. Ren, G. C. Schatz, T. Shegai, S. Schlücker, L.-L. Tay, K. G. Thomas, Z.-Q. Tian, R. P. Van Duyne, T. Vo-Dinh, Y. Wang, K. A. Willets, C. Xu, H. Xu, Y. Xu, Y. S. Yamamoto, B. Zhao and L. M. Liz-Marzán, *ACS Nano*, 2020, **14**, 28–117.
8 C. Zong, M. Xu, L.-J. Xu, T. Wei, X. Ma, X.-S. Zheng, R. Hu and B. Ren, *Chem. Rev.*, 2018, **118**, 4946–4980.
9 X. Wang, E. Zhang, H. Shi, Y. Tao and X. Ren, *Analyst*, 2022, **147**, 1257–1272.
10 X. Liu, J. Guo, Y. Li, B. Wang, S. Yang, W. Chen, X. Wu, J. Guo and X. Ma, *J. Mater. Chem. B*, 2021, **9**, 8378–8388.
11 Y. Hang, J. Boryczka and N. Wu, *Chem. Soc. Rev.*, 2022, **51**, 329–375.
12 S. Nie and S. R. Emory, *Science*, 1997, **275**, 1102–1106.
13 M. L. Thomas and P. Marcato, *Cancers*, 2018, **10**, 101.
14 K. Ng, A. Stenzl, A. Sharma and N. Vasdev, *Urol. Oncol.*, 2021, **39**, 41–51.
15 J. Marrugo-Ramírez, M. Mir and J. Samitier, *Int. J. Mol. Sci.*, 2018, **19**, 2877.
16 S. Chojnowska, I. Ptaszyńska-Sarosiek, A. Kępka, M. Knaś and N. Waszkiewicz, *J. Clin. Med.*, 2021, **10**, 517.
17 M. Russano, A. Napolitano, G. Ribelli, M. Iuliani, S. Simonetti, F. Citarella, F. Pantano, E. Dell'Aquila, C. Anesi, N. Silvestris, A. Argentiero, A. G. Solimando, B. Vincenzi, G. Tonini and D. Santini, *J. Exp. Clin. Cancer Res.*, 2020, **39**, 95.
18 G. Follain, D. Herrmann, S. Harlepp, V. Hyenne, N. Osmani, S. C. Warren, P. Timpson and J. G. Goetz, *Nat. Rev. Cancer*, 2020, **20**, 107–124.
19 P. Lewczuk, P. Riederer, S. E. O'Bryant, M. M. Verbeek, B. Dubois, P. J. Visser, K. A. Jellinger, S. Engelborghs, A. Ramirez, L. Parnetti, C. R. Jack, Jr., C. E. Teunissen, H. Hampel, A. Lleó, F. Jessen, L. Glodzik, M. J. de Leon, A. M. Fagan, J. L. Molinuevo, W. J. Jansen, B. Winblad, L. M. Shaw, U. Andreasson, M. Otto, B. Mollenhauer, J. Wiltfang, M. R. Turner, I. Zerr, R. Handels, A. G. Thompson, G. Johansson, N. Ermann, J. Q. Trojanowski, I. Karaca, H. Wagner, P. Oeckl, L. van Waalwijk van Doorn, M. Bjerke, D. Kapogiannis, H. B. Kuiperij, L. Farotti, Y. Li, B. A. Gordon, S. Epelbaum,

Published on 19 September 2022. Downloaded on 2026-01-07 6:31:26 nm..

S. J. B. Vos, C. J. M. Klijn, W. E. Van Nostrand, C. Minguillon, M. Schmitz, C. Gallo, A. Lopez Mato, F. Thibaut, S. Lista, D. Alcolea, H. Zetterberg, K. Blennow and J. Kornhuber, *World J. Biol. Psychiatry*, 2018, **19**, 244–328.
20 B. Pardini, A. A. Sabo, G. Birolo and G. A. Calin, *Cancers*, 2019, **11**, 1170.
21 B. Lei, Z. Tian, W. Fan and B. Ni, *Int. J. Med. Sci.*, 2019, **16**, 292–301.
22 E. Kilgour, D. G. Rothwell, G. Brady and C. Dive, *Cancer Cell*, 2020, **37**, 485–495.
23 J. Müller Bark, A. Kulasinghe, B. Chua, B. W. Day and C. Punyadeera, *Br. J. Cancer*, 2020, **122**, 295–305.
24 W. Yu, J. Hurley, D. Roberts, S. K. Chakrabortty, D. Enderle, M. Noerholm, X. O. Breakefield and J. K. Skog, *Ann. Oncol.*, 2021, **32**, 466–477.
25 H. Shao, H. Im, C. M. Castro, X. Breakefield, R. Weissleder and H. Lee, *Chem. Rev.*, 2018, **118**, 1917–1950.
26 A. Tukova and A. Rodger, *Emerging Top. Life Sci.*, 2021, **5**, 61–75.
27 T. Huang and C.-X. Deng, *Int. J. Biol. Sci.*, 2019, **15**, 1–11.
28 S. Wang, K. Zhang, S. Tan, J. Xin, Q. Yuan, H. Xu, X. Xu, Q. Liang, D. C. Christiani, M. Wang, L. Liu and M. Du, *Mol. Cancer*, 2021, **20**, 13.
29 C. Alix-Panabières and K. Pantel, *Cancer Discovery*, 2021, **11**, 858–873.
30 J. Lin, J. Zheng and A. Wu, *J. Mater. Chem. B*, 2020, **8**, 3316–3326.
31 J. Perumal, Y. Wang, A. B. E. Attia, U. S. Dinish and M. Olivo, *Nanoscale*, 2021, **13**, 553–580.
32 D. Cialla-May, X. S. Zheng, K. Weber and J. Popp, *Chem. Soc. Rev.*, 2017, **46**, 3945–3961.
33 L. K. Chin, T. Son, J.-S. Hong, A.-Q. Liu, J. Skog, C. M. Castro, R. Weissleder, H. Lee and H. Im, *ACS Nano*, 2020, **14**, 14528–14548.
34 Y. Zhang, X. Mi, X. Tan and R. Xiang, *Theranostics*, 2019, **9**, 491–525.
35 J. Wang, K. M. Koo, Y. Wang and M. Trau, *Adv. Sci.*, 2019, **6**, 1900730.
36 S. D. Christesen, *Appl. Spectrosc.*, 1988, **42**, 318–321.
37 M. Käll, H. Xu and P. Johansson, *J. Raman Spectrosc.*, 2005, **36**, 510–514.
38 S.-Y. Ding, J. Yi, J.-F. Li, B. Ren, D.-Y. Wu, R. Panneerselvam and Z.-Q. Tian, *Nat. Rev. Mater.*, 2016, **1**, 16021.
39 X. Wang and L. Guo, *Angew. Chem., Int. Ed.*, 2020, **59**, 4231–4239.
40 G. Mie, *Ann. Phys.*, 1908, **330**, 377–445.
41 X. Fan, W. Zheng and D. J. Singh, *Light: Sci. Appl.*, 2014, **3**, e179–e179.
42 K. M. Mayer and J. H. Hafner, *Chem. Rev.*, 2011, **111**, 3828–3857.
43 M. Tavakkoli Yaraki, Y. Pan, F. Hu, Y. Yu, B. Liu and Y. N. Tan, *Mater. Chem. Front.*, 2020, **4**, 3074–3085.
44 M. Tavakkoli Yaraki, F. Hu, S. Daqiqeh Rezaei, B. Liu and Y. N. Tan, *Nanoscale Adv.*, 2020, **2**, 2859–2869.
45 M. Tavakkoli Yaraki, S. Daqiqeh Rezaei and Y. N. Tan, *Phys. Chem. Chem. Phys.*, 2020, **22**, 5673–5687.
46 X. Zhang, H. Zhang, S. Yan, Z. Zeng, A. Huang, A. Liu, Y. Yuan and Y. Huang, *Sci. Rep.*, 2019, **9**, 17634.
47 P.-P. Fang, J.-F. Li, Z.-L. Yang, L.-M. Li, B. Ren and Z.-Q. Tian, *J. Raman Spectrosc.*, 2008, **39**, 1679–1687.
48 R. Kumar, L. Binetti, T. H. Nguyen, L. S. M. Alwis, A. Agrawal, T. Sun and K. T. V. Grattan, *Sci. Rep.*, 2019, **9**, 17469.
49 S. Hong and X. Li, *J. Nanomater.*, 2013, **2013**, 790323.
50 M. Tavakkoli Yaraki, S. Daqiqeh Rezaei, E. Middha and Y. N. Tan, *Part. Part. Syst. Charact.*, 2020, **37**, 2000027.
51 X. Liang, N. Li, R. Zhang, P. Yin, C. Zhang, N. Yang, K. Liang and B. Kong, *NPG Asia Mater.*, 2021, **13**, 8.
52 J. R. Lombardi and R. L. Birke, *J. Chem. Phys.*, 2007, **126**, 244709.
53 J. R. Lombardi and R. L. Birke, *J. Chem. Phys.*, 2012, **136**, 144704.
54 J. R. Lombardi and R. L. Birke, *J. Phys. Chem. C*, 2014, **118**, 11120–11130.
55 L. E. Brus, *J. Chem. Phys.*, 1984, **80**, 4403–4409.
56 T. Takagahara and K. Takeda, *Phys. Rev. B: Condens. Matter Mater. Phys.*, 1992, **46**, 15578–15581.
57 G. Song, W. Gong, S. Cong and Z. Zhao, *Angew. Chem., Int. Ed.*, 2021, **60**, 5505–5511.
58 G. Song, S. Cong and Z. Zhao, *Chem. Sci.*, 2022, **13**, 1210–1224.
59 L. Yang, Y. Peng, Y. Yang, J. Liu, H. Huang, B. Yu, J. Zhao, Y. Lu, Z. Huang, Z. Li and J. R. Lombardi, *Adv. Sci.*, 2019, **6**, 1900310.
60 Y. Liu, H. Ma, X. X. Han and B. Zhao, *Mater. Horiz.*, 2021, **8**, 370–382.
61 B. Yang, S. Jin, S. Guo, Y. Park, L. Chen, B. Zhao and Y. M. Jung, *ACS Omega*, 2019, **4**, 20101–20108.
62 Z. Zheng, S. Cong, W. Gong, J. Xuan, G. Li, W. Lu, F. Geng and Z. Zhao, *Nat. Commun.*, 2017, **8**, 1993.
63 S. Cong, X. Liu, Y. Jiang, W. Zhang and Z. Zhao, *Innovation*, 2020, **1**, 100051.
64 K. H. Lee, H. Jang, Y. S. Kim, C.-H. Lee, S. H. Cho, M. Kim, H. Son, K. B. Bae, D. V. Dao, Y. S. Jung and I.-H. Lee, *Adv. Sci.*, 2021, **8**, 2100640.
65 X. Jiang, X. Sun, D. Yin, X. Li, M. Yang, X. Han, L. Yang and B. Zhao, *Phys. Chem. Chem. Phys.*, 2017, **19**, 11212–11219.
66 Y. Peng, C. Lin, L. Long, T. Masaki, M. Tang, L. Yang, J. Liu, Z. Huang, Z. Li, X. Luo, J. R. Lombardi and Y. Yang, *Nano-Micro Lett.*, 2021, **13**, 52.
67 Y. Peng, C. Lin, Y. Li, Y. Gao, J. Wang, J. He, Z. Huang, J. Liu, X. Luo and Y. Yang, *Matter*, 2022, **5**, 694–709.
68 F. Avila, D. J. Fernandez, J. F. Arenas, J. C. Otero and J. Soto, *Chem. Commun.*, 2011, **47**, 4210–4212.
69 M. T. Yaraki and Y. N. Tan, *Chem. – Asian J.*, 2020, **15**, 3180–3208.

 This journal is © The Royal Society of Chemistry 2022

Published on 19 September 2022. Downloaded on 2026-01-07 6:31:26 nm..

70 H. Dong, Y. C. Chen and C. Feldmann, *Green Chem.*, 2015, **17**, 4107–4132.
71 R. Purbia and S. Paria, *Nanoscale*, 2015, **7**, 19789–19873.
72 F. Fiévet, S. Ammar-Merah, R. Brayner, F. Chau, M. Giraud, F. Mammeri, J. Peron, J. Y. Piquemal, L. Sicard and G. Viau, *Chem. Soc. Rev.*, 2018, **47**, 5187–5233.
73 H.-l. Liu, F. Nosheen and X. Wang, *Chem. Soc. Rev.*, 2015, **44**, 3056–3078.
74 M. Tavakkoli Yaraki and Y. N. Tan, *Sens. Int.*, 2020, **1**, 100049.
75 T. Zhang, X. Li, Y. Sun, D. Liu, C. Li, W. Cai and Y. Li, *Chem. Sci.*, 2021, **12**, 12631–12639.
76 M. A. Tahir, N. E. Dina, H. Cheng, V. K. Valev and L. Zhang, *Nanoscale*, 2021, **13**, 11593–11634.
77 L. W. Yap, H. Chen, Y. Gao, K. Petkovic, Y. Liang, K. J. Si, H. Wang, Z. Tang, Y. Zhu and W. Cheng, *Nanoscale*, 2017, **9**, 7822–7829.
78 Y. N. Tan, J. Y. Lee and D. I. C. Wang, *J. Phys. Chem. C*, 2008, **112**, 5463–5470.
79 Y.-N. Tan, J. Yang, J. Y. Lee and D. I. C. Wang, *J. Phys. Chem. C*, 2007, **111**, 14084–14090.
80 X. T. Zheng, H. V. Xu and Y. N. Tan, in *Advances in Bioinspired and Biomedical Materials Volume 2*, American Chemical Society, 2017, vol. 1253, ch. 7, pp. 123–152.
81 Y. N. Tan, J. Y. Lee and D. I. C. Wang, *J. Am. Chem. Soc.*, 2010, **132**, 5677–5686.
82 Y. N. Tan, J. Y. Lee and D. I. C. Wang, *J. Phys. Chem. C*, 2009, **113**, 10887–10895.
83 M. Mosaviniya, T. Kikhavani, M. Tanzifi, M. Tavakkoli Yaraki, P. Tajbakhsh and A. Lajevardi, *Colloid Interface Sci. Commun.*, 2019, **33**, 100211.
84 A. Nouri, M. Tavakkoli Yaraki, A. Lajevardi, Z. Rezaei, M. Ghorbanpour and M. Tanzifi, *Colloid Interface Sci. Commun.*, 2020, **35**, 100252.
85 K. Ijiro and H. Mitomo, *Polym. J.*, 2017, **49**, 815–824.
86 A. Tukova, I. C. Kuschnerus, A. Garcia-Bennett, Y. Wang and A. Rodger, *Nanomaterials*, 2021, **11**, 2565.
87 J. Li, G. Zhang, J. Wang, I. S. Maksymov, A. D. Greentree, J. Hu, A. Shen, Y. Wang and M. Trau, *ACS Appl. Mater. Interfaces*, 2018, **10**, 32526–32535.
88 Y. Sun and Y. Xia, *Science*, 2002, **298**, 2176–2179.
89 D. K. Smith and B. A. Korgel, *Langmuir*, 2008, **24**, 644–649.
90 S. Zhou, J. Li, K. D. Gilroy, J. Tao, C. Zhu, X. Yang, X. Sun and Y. Xia, *ACS Nano*, 2016, **10**, 9861–9870.
91 H. J. Kim, M. H. Lee, L. Mutihac, J. Vicens and J. S. Kim, *Chem. Soc. Rev.*, 2012, **41**, 1173–1190.
92 Y. Liu, Z. Lu, X. Lin, H. Zhu, W. Hasi, M. Zhang, X. Zhao and X. Lou, *RSC Adv.*, 2016, **6**, 58387–58393.
93 J. J. Mock, S. M. Norton, S. Y. Chen, A. A. Lazarides and D. R. Smith, *Plasmonics*, 2011, **6**, 113–124.
94 J. Liu, L. Chen, B. Duan, Z. Gu, Q. Luo and C. Duan, *RSC Adv.*, 2016, **6**, 38690–38696.
95 Q. He, A. Zhao, L. Li, H. Sun, D. Wang, H. Guo, M. Sun and P. Chen, *New J. Chem.*, 2017, **41**, 1582–1590.
96 D. M. Solís, J. M. Taboada, F. Obelleiro, L. M. Liz-Marzán and F. J. García de Abajo, *ACS Photonics*, 2017, **4**, 329–337.
97 M. Hu, F. S. Ou, W. Wu, I. Naumov, X. Li, A. M. Bratkovsky, R. S. Williams and Z. Li, *J. Am. Chem. Soc.*, 2010, **132**, 12820–12822.
98 X. Zhang, Y. Zheng, X. Liu, W. Lu, J. Dai, D. Y. Lei and D. R. MacFarlane, *Adv. Mater.*, 2015, **27**, 1090–1096.
99 Y. Chen, K. J. Si, D. Sikdar, Y. Tang, M. Premaratne and W. Cheng, *Adv. Opt. Mater.*, 2015, **3**, 919–924.
100 C. Hanske, E. H. Hill, D. Vila-Liarte, G. González-Rubio, C. Matricardi, A. Mihi and L. M. Liz-Marzán, *ACS Appl. Mater. Interfaces*, 2019, **11**, 11763–11771.
101 L. Song, J. Chen, B. B. Xu and Y. Huang, *ACS Nano*, 2021, **15**, 18822–18847.
102 H. Liu, J. Zeng, L. Song, L. Zhang, Z. Chen, J. Li, Z. Xiao, F. Su and Y. Huang, *Nanoscale Horiz.*, 2022, **7**, 554–561.
103 L. Song, B. B. Xu, Q. Cheng, X. Wang, X. Luo, X. Chen, T. Chen and Y. Huang, *Sci. Adv.*, 2021, **7**, eabk2852.
104 X. Lu, Y. Huang, B. Liu, L. Zhang, L. Song, J. Zhang, A. Zhang and T. Chen, *Chem. Mater.*, 2018, **30**, 1989–1997.
105 H. Yamada, Y. Yamamoto and N. Tani, *Chem. Phys. Lett.*, 1982, **86**, 397–400.
106 H. Yamada and Y. Yamamoto, *Surf. Sci.*, 1983, **134**, 71–90.
107 B. P. Majee, Bhawna and A. K. Mishra, *Mater. Res. Express*, 2020, **6**, 1250j1251.
108 J. Lin, J. Yu, O. U. Akakuru, X. Wang, B. Yuan, T. Chen, L. Guo and A. Wu, *Chem. Sci.*, 2020, **11**, 9414–9420.
109 E. Proniewicz, A. Tąta, A. Wójcik, M. Starowicz, J. Pacek and M. Molenda, *Phys. Chem. Chem. Phys.*, 2020, **22**, 28100–28114.
110 C. Liu, Q. Song, J. Chen, X. Li, J. Cai, Z. Lu, W. Li, N. X. Fang and S.-P. Feng, *Adv. Mater. Interfaces*, 2019, **6**, 1900534.
111 L. Yang, M. Gong, X. Jiang, D. Yin, X. Qin, B. Zhao and W. Ruan, *J. Raman Spectrosc.*, 2015, **46**, 287–292.
112 L. Yang, Y. Peng, Y. Yang, J. Liu, Z. Li, Y. Ma, Z. Zhang, Y. Wei, S. Li, Z. Huang and N. V. Long, *ACS Appl. Nano Mater.*, 2018, **1**, 4516–4527.
113 X. Xue, W. Ji, Z. Mao, H. Mao, Y. Wang, X. Wang, W. Ruan, B. Zhao and J. R. Lombardi, *J. Phys. Chem. C*, 2012, **116**, 8792–8797.
114 H. A. O. Wen, *Mol. Phys.*, 1996, **88**, 281–290.
115 H. Zhang, S. Huang, X. Yang, R. Yuan and Y. Chai, *Sens. Actuators, B*, 2021, **343**, 130142.
116 L. Yang, Y. Wei, Y. Song, Y. Peng, Y. Yang and Z. Huang, *Mater. Des.*, 2020, **193**, 108808.
117 X. Yan, Y. Ai-Hua, J. Wen-Qi and W. De-Ping, *Chin. J. Inorg. Chem.*, 2018, **34**, 1392–1398.
118 Z. Tian, H. Bai, C. Chen, Y. Ye, Q. Kong, Y. Li, W. Fan, W. Yi and G. Xi, *iScience*, 2019, **19**, 836–849.
119 Y. Li, R. Du, W. Li, J. Li, H. Yang, H. Bai, M. Zou and G. Xi, *Anal. Chem.*, 2021, **93**, 12360–12366.
120 Q. Zhang, X. Li, Q. Ma, Q. Zhang, H. Bai, W. Yi, J. Liu, J. Han and G. Xi, *Nat. Commun.*, 2017, **8**, 14903.
121 M. K. Patil, S. H. Gaikwad and S. P. Mukherjee, *J. Phys. Chem. C*, 2020, **124**, 21082–21093.
122 Y. Wang, W. Ruan, J. Zhang, B. Yang, W. Xu, B. Zhao and J. R. Lombardi, *J. Raman Spectrosc.*, 2009, **40**, 1072–1077.

Published on 19 September 2022. Downloaded on 2026-01-07 6:31:26 nm..

123 Y. Wang, H. Hu, S. Jing, Y. Wang, Z. Sun, B. Zhao, C. Zhao and J. R. Lombardi, *Anal. Sci.*, 2007, **23**, 787–791.
124 A. Li, J. Lin, Z. Huang, X. Wang and L. Guo, *iScience*, 2018, **10**, 1–10.
125 X. Wang, W. Shi, Z. Jin, W. Huang, J. Lin, G. Ma, S. Li and L. Guo, *Angew. Chem., Int. Ed.*, 2017, **56**, 9851–9855.
126 X. Wang, W. Shi, S. Wang, H. Zhao, J. Lin, Z. Yang, M. Chen and L. Guo, *J. Am. Chem. Soc.*, 2019, **141**, 5856–5862.
127 Y. Wang, Z. Sun, Y. Wang, H. Hu, B. Zhao, W. Xu and J. R. Lombardi, *Spectrochim. Acta, Part A*, 2007, **66**, 1199–1203.
128 M. Keshavarz, A. K. M. R. H. Chowdhury, P. Kassanos, B. Tan and K. Venkatakrishnan, *Sens. Actuators, B*, 2020, **323**, 128703.
129 S. Huh, J. Park, Y. S. Kim, K. S. Kim, B. H. Hong and J.-M. Nam, *ACS Nano*, 2011, **5**, 9799–9806.
130 D. Glass, E. Cortés, S. Ben-Jaber, T. Brick, W. J. Peveler, C. S. Blackman, C. R. Howle, R. Quesada-Cabrera, I. P. Parkin and S. A. Maier, *Adv. Sci.*, 2019, **6**, 1901841.
131 X. Zheng, F. Ren, S. Zhang, X. Zhang, H. Wu, X. Zhang, Z. Xing, W. Qin, Y. Liu and C. Jiang, *ACS Appl. Mater. Interfaces*, 2017, **9**, 14534–14544.
132 Y. Wang, M. Zhang, H. Ma, H. Su, A. Li, W. Ruan and B. Zhao, *ACS Appl. Mater. Interfaces*, 2021, **13**, 35038–35045.
133 J. Li, H. Bai, J. Zhai, W. Li, W. Fan and G. Xi, *Chem. Commun.*, 2019, **55**, 4679–4682.
134 Samriti, V. Rajput, R. K. Gupta and J. Prakash, *J. Mater. Chem. C*, 2022, **10**, 73–95.
135 H. Guan, Z. Tian, Q. Kong and G. Xi, *Chem. Commun.*, 2021, **57**, 4815–4818.
136 C. Gu, D. Li, S. Zeng, T. Jiang, X. Shen and H. Zhang, *Nanoscale*, 2021, **13**, 5620–5651.
137 Y. Peng, C. Lin, M. Tang, L. Yang, Y. Yang, J. Liu, Z. Huang and Z. Li, *Appl. Surf. Sci.*, 2020, **509**, 145376.
138 X. Pan, M.-Q. Yang, X. Fu, N. Zhang and Y.-J. Xu, *Nanoscale*, 2013, **5**, 3601–3614.
139 D. Luo, Z. Zhang, G. Li, S. Cheng, S. Li, J. Li, R. Gao, M. Li, S. Sy, Y.-P. Deng, Y. Jiang, Y. Zhu, H. Dou, Y. Hu, A. Yu and Z. Chen, *ACS Nano*, 2020, **14**, 4849–4860.
140 Y. Cao, P. Liang, Q. Dong, D. Wang, D. Zhang, L. Tang, L. Wang, S. Jin, D. Ni and Z. Yu, *Anal. Chem.*, 2019, **91**, 8683–8690.
141 X.-D. Zheng, F. Ren, H.-Y. Wu, W.-J. Qin and C.-Z. Jiang, *Nanotechnology*, 2018, **29**, 155301.
142 L. Kang, J. Chu, H. Zhao, P. Xu and M. Sun, *J. Mater. Chem. C*, 2015, **3**, 9024–9037.
143 H. Lai, F. Xu, Y. Zhang and L. Wang, *J. Mater. Chem. B*, 2018, **6**, 4008–4028.
144 M. D. Stoller, S. Park, Y. Zhu, J. An and R. S. Ruoff, *Nano Lett.*, 2008, **8**, 3498–3502.
145 M. C. Dalfovo, G. I. Lacconi, M. Moreno, M. C. Yappert, G. U. Sumanasekera, R. C. Salvarezza and F. J. Ibañez, *ACS Appl. Mater. Interfaces*, 2014, **6**, 6384–6391.
146 X. Ling, L. Xie, Y. Fang, H. Xu, H. Zhang, J. Kong, M. S. Dresselhaus, J. Zhang and Z. Liu, *Nano Lett.*, 2010, **10**, 553–561.
147 H. Xu, L. Xie, H. Zhang and J. Zhang, *ACS Nano*, 2011, **5**, 5338–5344.
148 H. Xu, Y. Chen, W. Xu, H. Zhang, J. Kong, M. S. Dresselhaus and J. Zhang, *Small*, 2011, **7**, 2945–2952.
149 X. Ling, J. Wu, W. Xu and J. Zhang, *Small*, 2012, **8**, 1365–1372.
150 F. Yin, S. Wu, Y. Wang, L. Wu, P. Yuan and X. Wang, *J. Solid State Chem.*, 2016, **237**, 57–63.
151 E. Er, H.-L. Hou, A. Criado, J. Langer, M. Möller, N. Erk, L. M. Liz-Marzán and M. Prato, *Chem. Mater.*, 2019, **31**, 5725–5734.
152 D. Yan, W. Qiu, X. Chen, L. Liu, Y. Lai, Z. Meng, J. Song, Y. Liu, X.-Y. Liu and D. Zhan, *J. Phys. Chem. C*, 2018, **122**, 14467–14473.
153 M. Li, Y. Gao, X. Fan, Y. Wei, Q. Hao and T. Qiu, *Nanoscale Horiz.*, 2021, **6**, 186–191.
154 C. Weng, Y. Luo, B. Wang, J. Shi, L. Gao, Z. Cao and G. Duan, *J. Mater. Chem. C*, 2020, **8**, 14138–14145.
155 L. Tao, K. Chen, Z. Chen, C. Cong, C. Qiu, J. Chen, X. Wang, H. Chen, T. Yu, W. Xie, S. Deng and J.-B. Xu, *J. Am. Chem. Soc.*, 2018, **140**, 8696–8704.
156 P. Miao, J.-K. Qin, Y. Shen, H. Su, J. Dai, B. Song, Y. Du, M. Sun, W. Zhang, H.-L. Wang, C.-Y. Xu and P. Xu, *Small*, 2018, **14**, 1704079.
157 P. Karthick Kannan, P. Shankar, C. Blackman and C.-H. Chung, *Adv. Mater.*, 2019, **31**, 1803432.
158 X. Ling, W. Fang, Y.-H. Lee, P. T. Araujo, X. Zhang, J. F. Rodriguez-Nieva, Y. Lin, J. Zhang, J. Kong and M. S. Dresselhaus, *Nano Lett.*, 2014, **14**, 3033–3040.
159 Y. Lee, H. Kim, J. Lee, S. H. Yu, E. Hwang, C. Lee, J.-H. Ahn and J. H. Cho, *Chem. Mater.*, 2016, **28**, 180–187.
160 L. Sun, H. Hu, D. Zhan, J. Yan, L. Liu, J. S. Teguh, E. K. L. Yeow, P. S. Lee and Z. Shen, *Small*, 2014, **10**, 1090–1095.
161 Z. Liu, S. Li, C. Hu, W. Zhang, H. Zhong and Z. Guo, *J. Raman Spectrosc.*, 2013, **44**, 75–80.
162 J. C. Reed, H. Zhu, A. Y. Zhu, C. Li and E. Cubukcu, *Nano Lett.*, 2012, **12**, 4090–4094.
163 V. Kaushik, H. L. Kagdada, D. K. Singh and S. Pathak, *Appl. Surf. Sci.*, 2022, **574**, 151724.
164 E. Er, A. Sánchez-Iglesias, A. Silvestri, B. Arnaiz, L. M. Liz-Marzán, M. Prato and A. Criado, *ACS Appl. Mater. Interfaces*, 2021, **13**, 8823–8831.
165 C. Lin, S. Liang, Y. Peng, L. Long, Y. Li, Z. Huang, N. V. Long, X. Luo, J. Liu, Z. Li and Y. Yang, *Nano-Micro Lett.*, 2022, **14**, 75.
166 W. Xu, X. Ling, J. Xiao, M. S. Dresselhaus, J. Kong, H. Xu, Z. Liu and J. Zhang, *Proc. Natl. Acad. Sci. U. S. A.*, 2012, **109**, 9281–9286.
167 P. Hoskin, T. Ajithkumar and V. Goh, *Imaging for Clinical Oncology*, Oxford University Press, 2021.
168 H. Brody, *Nature*, 2020, **579**, S1.

 This journal is © The Royal Society of Chemistry 2022

Published on 19 September 2022. Downloaded on 2026-01-07 6:31:26 nm..

169 M. Heinrich, L. Hofmann, H. Baurecht, P. M. Kreuzer, H. Knüttel, M. F. Leitzmann and C. Seliger, *Nat. Med.*, 2022, **28**, 852–859.
170 S. Haider, T. Azam, G. Leandro, H. Heinrich and H. Rumana, *Eye*, 2022, DOI: 10.1038/s41433-022-02185-1.
171 L. M. Almehmadi, S. M. Curley, N. A. Tokranova, S. A. Tenenbaum and I. K. Lednev, *Sci. Rep.*, 2019, **9**, 12356.
172 V. M. Szlag, R. S. Rodriguez, J. He, N. Hudson-Smith, H. Kang, N. Le, T. M. Reineke and C. L. Haynes, *ACS Appl. Mater. Interfaces*, 2018, **10**, 31825–31844.
173 Z. Wang, S. Zong, L. Wu, D. Zhu and Y. Cui, *Chem. Rev.*, 2017, **117**, 7910–7963.
174 M. Bhamidipati, H.-Y. Cho, K.-B. Lee and L. Fabris, *Bioconjugate Chem.*, 2018, **29**, 2970–2981.
175 K. M. Koo, J. Wang, R. S. Richards, A. Farrell, J. W. Yaxley, H. Samaratunga, P. E. Teloken, M. J. Roberts, G. D. Coughlin, M. F. Lavin, P. N. Mainwaring, Y. Wang, R. A. Gardiner and M. Trau, *ACS Nano*, 2018, **12**, 8362–8371.
176 Y. Yang, C. Song, J. Zhang, J. Chao, H. M. Luong, Y. Zhao and L. Wang, *Nanoscale*, 2022, **14**, 4538–4547.
177 Y. Liu, N. Lyu, A. Rodger and Y. Wang, in *Principles and Clinical Diagnostic Applications of Surface-Enhanced Raman Spectroscopy*, ed. Y. Wang, Elsevier, 2022, pp. 225–280, DOI: 10.1016/B978-0-12-821121-2.00008-1.
178 W. Zhang, L. Wang, D. Li, D. H. Campbell, B. J. Walsh, N. H. Packer, Q. Dong, E. Wang and Y. Wang, *Anal. Methods*, 2022, **14**, 2255–2265.
179 K. B. Shanmugasundaram, J. Li, A. I. Sina, A. Wuethrich and M. Trau, *Mater. Adv.*, 2022, **3**, 1459–1471.
180 A. Khalifa and D. C. Rockey, *Curr. Opin. Gastroenterol.*, 2020, **36**, 184–191.
181 B. Salzman, E. Collins and L. Hersh, *Am. Fam. Physician*, 2019, **99**, 505–514.
182 J. Streicher, B. L. Meyerson, V. Karivedu and A. Sidana, *Ther. Adv. Urol.*, 2019, **11**, 1–8.
183 H. Liu, X. Gao, C. Xu and D. Liu, *Theranostics*, 2022, **12**, 1870–1903.
184 W. Zhang, L. Jiang, R. J. Diefenbach, D. H. Campbell, B. J. Walsh, N. H. Packer and Y. Wang, *ACS Sens.*, 2020, **5**, 764–771.
185 J. Wang, Y.-C. Kao, Q. Zhou, A. Wuethrich, M. S. Stark, H. Schaider, H. P. Soyer, L. L. Lin and M. Trau, *Adv. Funct. Mater.*, 2022, **32**, 2010296.
186 S. Jiang, Q. Li, C. Wang, Y. Pang, Z. Sun and R. Xiao, *ACS Sens.*, 2021, **6**, 852–862.
187 F. Beffara, J. Perumal, A. Puteri Mahyuddin, M. Choolani, S. A. Khan, J. L. Auguste, S. Vedraine, G. Humbert, U. S. Dinish and M. Olivo, *J. Biophotonics*, 2020, **13**, e201960120.
188 H. Shin, D. Seo and Y. Choi, *Molecules*, 2020, **25**, 5209.
189 L. Guerrini, E. Garcia-Rico, A. O'Loghlen, V. Giannini and R. A. Alvarez-Puebla, *Cancers*, 2021, **13**, 2179.
190 S. C.-H. Tsao, J. Wang, Y. Wang, A. Behren, J. Cebon and M. Trau, *Nat. Commun.*, 2018, **9**, 1482.
191 S. Schlücker, *World Scientific Reference on Plasmonic Nanomaterials*, 2022, https://www.worldscientific.com/doi/10.1142/12236-vol5#t=aboutBook.
192 G. Sanità, B. Carrese and A. Lamberti, *Front. Mol. Biosci.*, 2020, **7**, 587012.
193 N. M. Cordina, W. Zhang, N. H. Packer and Y. Wang, *Mol. Omics*, 2020, **16**, 339–344.
194 N. Lyu, B. Pedersen, E. Shklovskaya, H. Rizos, M. P. Molloy and Y. Wang, *Exploration*, 2022, **2**, 20210176.
195 J. Li, A. Wuethrich, A. A. I. Sina, H.-H. Cheng, Y. Wang, A. Behren, P. N. Mainwaring and M. Trau, *Nat. Commun.*, 2021, **12**, 1087.
196 J. Wang, A. Wuethrich, A. A. I. Sina, R. E. Lane, L. L. Lin, Y. Wang, J. Cebon, A. Behren and M. Trau, *Sci. Adv.*, 2020, **6**, eaax3223.
197 J. Wang, W. Anderson, J. Li, L. L. Lin, Y. Wang and M. Trau, *J. Colloid Interface Sci.*, 2019, **537**, 536–546.
198 R. Mei, Y. Wang, X. Zhao, Q. Kang, D. Shen and L. Chen, *Anal. Chem.*, 2021, **93**, 16590–16597.
199 D. Song, R. Yang, S. Fang, Y. Liu, F. Long and A. Zhu, *Microchim. Acta*, 2018, **185**, 491.
200 S. Juergensen, P. Kusch and S. Reich, *Phys. Status Solidi B*, 2020, **257**, 2000295.
201 H. Y. Lau, Y. Wang, E. J. H. Wee, J. R. Botella and M. Trau, *Anal. Chem.*, 2016, **88**, 8074–8081.
202 J. Ye, J. A. Hutchison, H. Uji-i, J. Hofkens, L. Lagae, G. Maes, G. Borghs and P. Van Dorpe, *Nanoscale*, 2012, **4**, 1606–1611.
203 A. Mao, X. Jin, X. Gu, X. Wei and G. Yang, *J. Mol. Struct.*, 2012, **1021**, 158–161.
204 C. H. Sun, M. L. Wang, Q. Feng, W. Liu and C. X. Xu, *Russ. J. Phys. Chem. A*, 2015, **89**, 291–296.
205 C. Li, Y. Huang, K. Lai, B. A. Rasco and Y. Fan, *Food Control*, 2016, **65**, 99–105.
206 Y. Zeng, J.-Q. Ren, A.-G. Shen and J.-M. Hu, *J. Am. Chem. Soc.*, 2018, **140**, 10649–10652.
207 G. Fan, X. Gao, S. Xu, X. Li, Q. Zhang, C. Dai, Q. Xue and H. Wang, *Chem. Commun.*, 2022, **58**, 407–410.
208 D. Lu, M. Ran, Y. Liu, J. Xia, L. Bi and X. Cao, *Anal. Bioanal. Chem.*, 2020, **412**, 7099–7112.
209 Y. T. Yang, I. L. Hsu, T. Y. Cheng, W. J. Wu, C. W. Lee, T. J. Li, C. I. Cheung, Y. C. Chin, H. C. Chen, Y. C. Chiu, C. C. Huang and M. Y. Liao, *Anal. Chem.*, 2019, **91**, 8213–8220.
210 H. Wen, H. Wang, J. Hai, S. He, F. Chen and B. Wang, *ACS Sustainable Chem. Eng.*, 2019, **7**, 5200–5208.
211 C. Fan, N. Zhao, K. Cui, G. Chen, Y. Chen, W. Wu, Q. Li, Y. Cui, R. Li and Z. Xiao, *ACS Sens.*, 2021, **6**, 3234–3241.
212 M. Hou, D. He, H. Bu, H. Wang, J. Huang, J. Gu, R. Wu, H.-W. Li, X. He and K. Wang, *Analyst*, 2020, **145**, 6232–6236.
213 M. Muhammad, C.-S. Shao, C. Liu and Q. Huang, *ACS Appl. Bio Mater.*, 2021, **4**, 8386–8395.
214 K. K. Reza, S. Dey, A. Wuethrich, W. Jing, A. Behren, F. Antaw, Y. Wang, A. A. I. Sina and M. Trau, *ACS Nano*, 2021, **15**, 11231–11243.

Published on 19 September 2022. Downloaded on 2026-01-07 6:31:26 nm..

215 J. Wang, A. Wuethrich, R. J. Lobb, F. Antaw, A. A. Sina, R. E. Lane, Q. Zhou, C. Zieschank, C. Bell, V. F. Bonazzi, L. G. Aoude, S. Everitt, B. Yeo, A. P. Barbour, A. Möller and M. Trau, *ACS Sens.*, 2021, **6**, 3182–3194.
216 Y. Pang, J. Shi, X. Yang, C. Wang, Z. Sun and R. Xiao, *Biosens. Bioelectron.*, 2020, **148**, 111800.
217 Y. Xu, D. Zhang, J. Lin, X. Wu, X. Xu, O. U. Akakuru, H. Zhang, Z. Zhang, Y. Xie, A. Wu and G. Shao, *Biomater. Sci.*, 2022, **10**, 1812–1820.
218 J. He, J. Dong, Y. Hu, G. Li and Y. Hu, *Nanoscale*, 2019, **11**, 6089–6100.
219 Q. Lv, H. Min, D.-B. Duan, W. Fang, G.-M. Pan, A.-G. Shen, Q.-Q. Wang, G. Nie and J.-M. Hu, *Adv. Healthcare Mater.*, 2019, **8**, 1801257.
220 J. Lu, W. Zhang, H. Wang, Y. Mao, D. Di, Q. Zhao and S. Wang, *Colloids Surf., A*, 2020, **603**, 125212.
221 Y. Zhu, Q. Sun, Y. Liu, T. Ma, L. Su, S. Liu, X. Shi, D. Han and F. Liang, *R. Soc. Open Sci.*, 2018, **5**, 180159.
222 M. Z. Quazi, U. Lee, S. Park, S. Shin, E. Sim, H. Son and N. Park, *ACS Appl. Bio Mater.*, 2021, **4**, 8377–8385.
223 A. Das, V. Arunagiri, H.-C. Tsai, A. Prasannan and R. S. Moirangthem, *ACS Appl. Nano Mater.*, 2021, **4**, 12278–12288.
224 P. T. Sujai, S. Shamjith, M. M. Joseph and K. K. Maiti, *ACS Appl. Bio Mater.*, 2021, **4**, 4962–4972.
225 J. Lin, W. Ren, A. Li, C. Yao, T. Chen, X. Ma, X. Wang and A. Wu, *ACS Appl. Mater. Interfaces*, 2020, **12**, 4204–4211.
226 O. M. Elsharkasy, J. Z. Nordin, D. W. Hagey, O. G. de Jong, R. M. Schiffelers, S. E. Andaloussi and P. Vader, *Adv. Drug Delivery Rev.*, 2020, **159**, 332–343.
227 X. Zhang, H. Zhang, J. Gu, J. Zhang, H. Shi, H. Qian, D. Wang, W. Xu, J. Pan and H. A. Santos, *Adv. Mater.*, 2021, **33**, 2005709.
228 R. Haldavnekar, K. Venkatakrishnan and D. B. Tan, *Biosens. Bioelectron.*, 2021, **190**, 113407.
229 N. M. Ćulum, T. T. Cooper, G. I. Bell, D. A. Hess and F. Lagugné-Labarthet, *Anal. Bioanal. Chem.*, 2021, **413**, 5013–5024.
230 S. K. Das, K. Pal, T. S. Bhattacharya, P. Karmakar and J. Chowdhury, *Sens. Actuators, B*, 2019, **299**, 126962.
231 J. C. Fraire, S. Stremersch, D. Bouckaert, T. Monteyne, T. De Beer, P. Wuytens, R. De Rycke, A. G. Skirtach, K. Raemdonck, S. De Smedt and K. Braeckmans, *ACS Appl. Mater. Interfaces*, 2019, **11**, 39424–39435.
232 Y. Liu, W. Zhang, T. H. Phan, W. Chrzanowski, A. Rodger and Y. Wang, *Anal. Methods*, 2020, **12**, 5908–5915.
233 H. J. Koster, T. Rojalin, A. Powell, D. Pham, R. R. Mizenko, A. C. Birkeland and R. P. Carney, *Nanoscale*, 2021, **13**, 14760–14776.
234 N. Cheng, J. Fu, D. Chen, S. Chen and H. Wang, *NanoImpact*, 2021, **21**, 100296.
235 M. Erzina, A. Trelin, O. Guselnikova, B. Dvorankova, K. Strnadova, A. Perminova, P. Ulbrich, D. Mares, V. Jerabek, R. Elashnikov, V. Svorcik and O. Lyutakov, *Sens. Actuators, B*, 2020, **308**, 127660.
236 X. Ren, W. Nam, P. Ghassemi, J. S. Strobl, I. Kim, W. Zhou and M. Agah, *Microsyst. Nanoeng.*, 2020, **6**, 47.
237 M. Jue, C.-G. Pack, S. Oh, B. Paulson, K. Lee and J. K. Kim, *Materials*, 2020, **13**, 5321.
238 T.-H. Chang, K.-W. Chuang and Y.-C. Chang, *J. Alloys Compd.*, 2022, **893**, 162288.
239 P. Yin, G. Li, B. Zhang, H. Farjana, L. Zhao, H. Qin, B. Hu, J. Ou and J. Tian, *Analyst*, 2021, **146**, 1949–1955.
240 A. K. Ludwig, K. De Miroschedji, T. R. Doeppner, V. Börger, J. Ruesing, V. Rebmann, S. Durst, S. Jansen, M. Bremer, E. Behrmann, B. B. Singer, H. Jastrow, J. D. Kuhlmann, F. El Magraoui, H. E. Meyer, D. M. Hermann, B. Opalka, S. Raunser, M. Epple, P. A. Horn and B. Giebel, *J. Extracell. Vesicles*, 2018, **7**, 1528109.
241 M. A. Rider, S. N. Hurwitz and D. G. Meckes, *Sci. Rep.*, 2016, **6**, 23978.
242 F. Haque, A. Zavabeti, B. Y. Zhang, R. S. Datta, Y. Yin, Z. Yi, Y. Wang, N. Mahmood, N. Pillai, N. Syed, H. Khan, A. Jannat, N. Wang, N. Medhekar, K. Kalantar-zadeh and J. Z. Ou, *J. Mater. Chem. A*, 2019, **7**, 257–268.
243 B. Y. Zhang, P. Yin, Y. Hu, C. Szydzik, M. W. Khan, K. Xu, P. Thurgood, N. Mahmood, C. Dekiwadia, S. Afrin, Y. Yang, Q. Ma, C. F. McConville, K. Khoshmanesh, A. Mitchell, B. Hu, S. Baratchi and J. Z. Ou, *Biosens. Bioelectron.*, 2022, **198**, 113814.
244 Z. Yan, S. Dutta, Z. Liu, X. Yu, N. Mesgarzadeh, F. Ji, G. Bitan and Y.-H. Xie, *ACS Sens.*, 2019, **4**, 488–497.
245 S. Adesoye and K. Dellinger, *Sens. Biosensing Res.*, 2022, **37**, 100499.

 This journal is © The Royal Society of Chemistry 2022